A MATHEMATICAL MODEL BASED ANALYSIS FOR DESIGNING DEMO SCALE FUEL PROCESSOR

by

Barış Demirci

B.S., Chemical Engineering, Boğaziçi University, 2014

Submitted to the Institute for Graduate Studies in
Science and Engineering in partial fulfillment of
the requirements for the degree of
Master of Science

Graduate Program in Chemical Engineering
Boğaziçi University
2017

A MATHEMATICAL MODEL BASED ANALYSIS FOR DESIGNING DEMO SCALE FUEL PROCESSOR

APPROVED BY:

Prof. Ahmet Erhan AKSOYLU (Thesis Supervisor)	……
Assist. Prof. Hasan BEDİR (Thesis Co-supervisor)	……..……...
Prof. Ramazan Yıldırım	……
Prof. Hüsnü Atakül	……
Assoc. Prof. Alper Uzun	……

DATE OF APPROVAL: 01.08.2017

to my family

ACKNOWLEDGEMENTS

First of all, I would like to express my deep gratitude to my thesis supervisor Prof. Ahmet Erhan Aksoylu for his guidance, encouragement and trust in me. I also would like to thank my thesis co-supervisor Assoc. Prof. Hasan Bedir for his support and wisdom in modeling the system. It was a great privilege for me to work with them, where I learned from their great expertise and experiences in reaction engineering and modeling.

Very special thanks to Burcu Selen Çağlayan for her everlasting help and guidance throughout my work.

I am truly grateful to Prof. Ramazan Yıldırım, Prof. Hüsnü Atakül and Assoc. Prof. Alper Uzun for accepting to be a member of my thesis committee, sparing their time for reading and commenting on my thesis.

My greatest gratitude goes to Melek Selcen Başar for her patience, guidance and wisdom throughout my work. She greatly helped me as if she was my second co-supervisor. She was always eager to help me when I needed the most.

All our research team; Burcu Acar, Özgü Özer, Bahar Kesim, Gizem Yumru, Merve Eropak, Ali Uzun, Serhat Erşahin, Gözde Öztürk, Cihat Öztepe, Elif Erdinç, Ipek Paksoy and Gülşah Gül deserve my heartfelt thanks for their contribution and help in writing my thesis.

I would like to thank all members of KB 405 for their support and friendship. I also would like to thank all team members and my colleagues in CATREL and ChE Department.

Finally, I would like to express my dearest gratitude to my beloved family for their encouragement and moral support throughout my life. This is why I dedicate this work to them.

Financial support for this study was provided by TÜBİTAK through project 215M312. The financial support provided for lab infrastructure by Republic of Turkey Ministry of Development through project 2016K121160 is greatly acknowledged.

ABSTRACT

A MATHEMATICAL MODEL BASED ANALYSIS FOR DESIGNING DEMO SCALE FUEL PROCESSOR

The aim of this study is to construct a FLUENT-based mathematical model of a Demo-scale fuel processor, which will be used as the base model to obtain the optimum operating parameters of a Demo-FP that produces sufficient amount of PEM-grade H_2, having CO concentration below 100 ppm, from methane in amount enough to feed a 1 kW PEMFC. In the first part, the power law type kinetic expressions obtained from kinetic studies for the FP reactions (OSR-WGS-PROX) were corrected through minimizing the difference between experimentally obtained performance test results and the results obtained from the mathematical model formed in the current study for the same reaction conditions. In the second part, the fuel processor prototype (FPP) was modeled and its performance was simulated through the use of corrected kinetic models. 16 FPP simulations of the OSR reactor were performed by using the feed composition, temperature and W/F used in the first part. First, FP reactors having ¼ inch-OD were modeled in series. Then, the same simulations were performed for 1 inch-OD of the reactors, which is the OD of the reactors has been planned to be used in Demo-FP, while the catalyst bed height of each reactor were kept fixed as in the case of ¼ inch reactors; in those simulations, the catalyst amount and the flow rate of the OSR feed was increased such as to keep W/F of the OSR reactor the same as that of the ¼ inch reactor case. Finally, the reaction conditions yielding the best performance in terms of H_2 and CO level at the PROX outlet (*the simulations with 400 ^oC OSR reactor temperature*) were selected. For the selected sets, the catalyst amounts in the reactors increased while keeping the W/F fixed such as to satisfy the H_2 flow of 0.00272 moles/s and CO concentration of 100 ppm. In the last part, the operation of individual OSR reactor was further simulated for granule-size technical catalyst via introducing several levels of effectiveness factor to the power-law type OSR kinetic expression. The required catalyst amounts and the pressure drop values for the particle diameters and effectiveness factors studied were calculated. The bed density change with the change in particle size was almost insignificant, and consequently almost the same bed lengths were found. On the other hand, as the particle diameter was increased, the pressure drop was reduced sharply.

ÖZET

DEMO ÖLÇEKLİ YAKIT İŞLEMCI DİZAYNI İÇİN MATEMATİKSEL MODEL MERKEZLİ ANALİZ

Bu çalışmanın amacı, 1 kW'lık bir PEMFC beslemek için metandan yeterli miktarda PEM-dereceli H_2 üreten, 100 ppm'nin altında CO konsantrasyonuna sahip olan bir demo yakıt işlemcisinin optimum çalışma parametrelerini elde etmek için taban model olarak kullanılacak demo-ölçekli yakıt işlemcisinin FLUENT temelli bir matematiksel modeli oluşturmaktır. Birinci bölümde, aynı reaksiyon koşulları için deneysel olarak elde edilen performans testi sonuçları ile mevcut çalışmadan elde edilen matematiksel model sonuçları arasındaki farkın asgariye indirilmesi için, FP reaksiyonları (OSR-WGS-PROX) için kinetik araştırmalardan elde edilen güç yasası tipi kinetik ifadeler düzeltildi. İkinci bölümde, yakıt işlemci prototipi (FPP) modellendi ve performansı, düzeltilmiş kinetik modeller kullanılarak simüle edildi. OSR reaktörünün FPP simülasyonları ilk bölümde kullanılan giriş kompozisyonu, sıcaklık ve W/F kullanılarak gerçekleştirildi. İlk olarak, ¼ inç dış çaplı FP reaktörler seri olarak modellendi. Ardından, aynı simülasyonlar, her reaktörün katalizatör yatağı yüksekliği, 1/4 inç reaktörlerinkiyle aynı tutulacak şekilde, Demo-FP'de kullanılacak olan reaktörlerin dış çapı olması planlanan 1 inç dış çaplı reaktörler için gerçekleştirildi. Bu simülasyonlarda, katalizör miktarı ve OSR girişinin akış hızı, OSR reaktörünün W/F oranının ¼ inçlik reaktördeki ile aynı kalacak şekilde arttırılmıştır. Son olarak, PROX reaktör çıkışında H_2 üretimi ve CO seviyesi açısından en iyi performansı veren reaksiyon koşulları (*400 ^oC OSR reaktör sıcaklığına sahip olan simülasyonlar*) seçildi. Bu dört seçilmiş set için, reaktördeki katalizör miktarı; 0.00272 mol/sn H_2 akışını ve 100 ppm CO konsantrasyonunu karşılayacak şekilde W/F oranını sabit tutarak arttırıldı. Son bölümde, OSR reaktörünün çalışması, güç yasası tipi OSR kinetik ifadesine çeşitli düzeylerde etkinlik faktörleri ekleyerek granül boyutlu teknik katalizör için de simüle edildi. Çalışılan parçacık çapları ve etkinlik faktörleri için gereken katalizör miktarları ve basınç düşüş değerleri hesaplandı. Parçacık büyüklüğündeki değişimden ötürü meydana gelen yatak yoğunluğundaki değişimin neredeyse önemsiz olduğu gözlenmiş ve dolayısıyla hemen hemen aynı yatak uzunlukları bulunmuştur. Öte yandan, parçacık çapı arttıkça, basınç düşmesi keskin bir şekilde azalmıştır.

TABLE OF CONTENTS

ACKNOWLEDGEMENTS iv

ABSTRACT v

ÖZET vi

LIST OF FIGURES ix

LIST OF TABLES x

LIST OF SYMBOLS xiv

LIST OF ACRONYMS/ABBREVIATIONS xvi

1. INTRODUCTION 1

2. LITERATURE SURVEY 4

2.1. Decentralized Energy Production 4

2.2. Fuel Cells 4

2.3. Hydrogen 5

2.4. Fuel Processors 6

2.5. Reforming Reactions 6

2.5.1. Steam Reforming 7

2.5.2. Partial (POX) and Total (TOX) Oxidation 7

2.5.3. Oxidative Steam (OSR) and Autothermal (ATR) Reforming 8

2.6. Water Gas Shift (WGS) Reaction 10

2.7. Preferential Oxidation (PROX) Reaction 11

2.8. Fluid Flow in Porous Media 13

2.8.1. Reynolds Number and Flow Regimes 13

2.8.2. Porosity 14

2.8.3. Permeability 15

2.8.4. Inertial Resistance 16

2.8.5. Ergun Equation 16
2.8.6. Effectiveness Factor 17
2.9. Modeling of Fuel Processor Reactions 18
3. CALCULATIONS 23
3.1. ANSYS Fluent Simulations 23
3.1.1. Creating the Geometry 23
3.1.2. Meshing the Geometry 25
3.1.3. Fluent 26
3.2. Polymath Calculations 27
4. RESULTS AND DISCUSSION 30
4.1. Modeling of Performance Tests and Validating Kinetic Expressions 30
4.1.1. OSR Performance Tests 31
4.1.2. WGS Performance Tests 42
4.1.3. PROX Performance Tests 46
4.2. Modeling of Fuel Processor System 49
4.2.1. Fuel Processor System with 0.25 Inch Reactor Diameter 50
4.2.2. Demo-Fuel Processor System with 1 Inch Reactor Diameter 56
4.3. Modeling of OSR: Effect of Catalyst Size and Effectiveness Factor 62
5. CONCLUSION 69
5.1. Conclusions 69
5.2. Recommendations 71
REFERENCES 72

LIST OF FIGURES

Figure 2.1. Schematic of an individual fuel cell (EG&G Technical Services, Inc., 2004) 5

Figure 2.2. Schematic of a simple fuel processor (Salemme *et al.*, 2010) 6

Figure 3.1. Modeled geometry of a reactor 24

Figure 3.2. Modeled geometry of a fuel processor unit 25

Figure 3.3. Cells created by ANSYS Meshing 26

Figure 3.4 ANSYS Fluent 26

Figure 4.1. PROX performance of Pt–Sn/AC-N as CO conversion at O_2:CO = 1:1 (Çağlayan *et al.*, 2011) 51

Figure 4.2. H_2 outlet concentration from different reactors in fuel processor system with 1-inch reactor diameter 60

Figure 4.3. H_2 outlet concentration from different reactors in fuel processor system with 1-inch reactor diameter 61

Figure 4.4. Catalyst bed length for different particle diameters 66

Figure 4.5. Pressure drop for different particle diameters 67

LIST OF TABLES

Table 3.1. Specifications of reactor used in experiments 23

Table 3.2. Densities of catalyst used in FP reactions 24

Table 4.1. Estimated rate parameters for methane OSR over 0.2Pt-10Ni/δ-Al_2O_3 catalyst (Erdinç, 2014)..... 32

Table 4.2. Modified rate expression parameters for methane OSR over 0.2Pt-10Ni/δ-Al_2O_3 catalyst 32

Table 4.3. Main reactions take place in OSR reactor 33

Table 4.4. List of performance test parameters over 0.2Pt-10Ni/δ-Al_2O_3 catalyst..... 34

Table 4.5. List of performance tests over 0.2Pt-10Ni/δ-Al_2O_3 catalyst (Başar *et al.*) 35

Table 4.6. List of stoichiometric coefficients of performance tests 36

Table 4.7. Fluent and Polymath CH_4 conversion results of performance tests over 0.2Pt-10Ni/δ-Al_2O_3 catalyst..... 37

Table 4.8. Fluent and Polymath H_2 production results of performance tests over 0.2Pt-10Ni/δ-Al_2O_3 catalyst..... 38

Table 4.9. Porous body parameters of 0.2Pt-10Ni/δ-Al_2O_3 catalyst..... 39

Table 4.10. Fluent H_2 production and CH_4 conversion with 1.5 correction factor and porous body parameters results of performance tests over 0.2Pt-10Ni/δ-Al_2O_3 catalyst..... 40

Table 4.11. Fluent outlet composition of CO results of performance tests over 0.2Pt-10Ni/δ-Al_2O_3 catalyst 41

Table 4.12. Estimated rate expression parameters over 1Pt-0.5Re-1V/CeO_2 catalyst (Yumru, 2017) 43

Table 4.13. Modified rate expression parameters over 1Pt-0.5Re-1V/CeO_2 catalyst... 43

Table 4.14. List of performance tests over 1Pt-0.5Re-1V/CeO_2 catalyst (Kesim, 2017)..... 44

Table 4.15. List of performance tests over 1Pt-0.5Re-1V/CeO_2 catalyst 44

Table 4.16. Fluent and Polymath CO conversion results of performance tests over 1Pt-0.5Re-1V/CeO_2 catalyst 44

Table 4.17. Porous body parameters of 1Pt-0.5Re-1V/CeO_2 catalyst 45

Table 4.18. Fluent CO conversion with 0.33 correction factor and porous body parameters results of performance tests over 1Pt-0.5Re-1V/CeO_2 catalyst 45

Table 4.19. Estimated rate expression parameters over 1Pt-0.25Sn/AC catalyst (Eropak and Aksoylu, 2017)..... 46

Table 4.20. Modified rate expression parameters over 1Pt-0.25Sn/AC catalyst..... 47

Table 4.21. List of performance tests over 1Pt-0.25Sn/AC catalyst (Çağlayan *et al.*, 2011)..... 47

Table 4.22. List of performance tests over 1Pt-0.25Sn/AC catalyst 48

Table 4.23. Fluent and Polymath CO conversion results of performance tests over 1Pt-0.25Sn/AC catalyst..... 48

Table 4.24. Porous body parameters of 1Pt-0.25Sn/AC catalyst..... 48

Table 4.25. Fluent CO conversion with porous body parameters results of performance tests over 1Pt-0.25Sn/AC catalyst 49

Table 4.26. Outlet compositions of OSR performance tests over 0.2Pt-10Ni/δ-Al_2O_3 catalyst and (1-β') factors for WGS reaction over 1Pt-0.5Re-1V/CeO_2 catalyst 52

Table 4.27. Specifications of the FPP system utilizing 0.25-inch OD reactors 53

Table 4.28. Inlet compositions and OSR temperature of the FPP system utilizing 0.25-inch OD reactors..... 54

Table 4.29. Results of the fuel processor system with 0.25-inch reactor diameter 55

Table 4.30. Specifications of the DFP system with 1-inch reactor diameter 57

Table 4.31. Inlet compositions and OSR temperature of the DFP system with 1-inch reactor diameter 58

Table 4.32. Results of the fuel processor system with 1-inch reactor diameter 59

Table 4.33. Required OSR catalyst weights to feed 1kW PEMFC 61

Table 4.34. Required WGS catalyst weights to feed 1kW PEMFC 62

Table 4.35. Required PROX catalyst weights to feed 1kW PEMFC 62

Table 4.36. Effectiveness factor for different particle diameters 64

Table 4.37. Effect of particle diameter to the catalyst weight and pressure drop with 1 effectiveness factor 65

Table 4.38. Effect of particle diameter to the catalyst weight and pressure drop with 0.6 effectiveness factor 65

Table 4.39. Effect of effectiveness factor to the catalyst weight and pressure drop with 0.7 μm particle diameter 66

Table 4.40. Effect of effectiveness factor to the catalyst weight and pressure drop with 0.5 μm particle diameter 67

LIST OF SYMBOLS

A	Cross-sectional area
C	Inertial resistance
C	Concentration
D	Characteristic length
d_p	Particle diameter
D_r	Reactor diameter
E_A	Activation energy
F	Flow rate
k_0	Pre-exponential factor
K	Permeability
K_c	Kozeny constant
L	Bed length
N	Number of moles
P	Pressure drop
R	Reaction rate
R	Gas constant
Re	Reynolds number
S_p	Surface area of particle
S_v	Specific surface
T	Temperature
U	Flow rate of the fluid
V	Volume
V_p	Volume of particle
X	Mole fraction
X	Conversion
W	Catalyst weight
α	Rate order of CH_4 in OSR, CO in WGS and CO in PROX reactions
β	Rate order of O_2 in OSR, H_2O in WGS and O_2 in PROX reactions

β'	Beta factor
γ	Rate order of H_2O in OSR, H_2 in WGS reactions
δ	Rate order of CO_2 in WGS reaction
ε	Porosity, Rate order of CH_4 in WGS reaction
η	Effectiveness factor
μ	Dynamic viscosity
ξ	Extent of reaction
ρ	Density
ρ_b	Bulk density
ρ_s	Solid density
τ	Tortuosity
φ	Stoichiometric coefficient
i	Species
in	Inlet
j	Reaction
out	Outlet

LIST OF ACRONYMS/ABBREVIATIONS

AC-N	Activated Carbon
AFC	Alkaline Fuel Cells
ATR	Autothermal Reforming
CDF	Computational Fluid Dynamics
CSTR	Continuous Stirred Tank Reactor
DFP	Demo-Scale Fuel Processor
DMFC	Direct Methanol Fuel Cells
FC	Fuel Cell
FP	Fuel Processor
FPP	Fuel Processor Prototype
HTS	High Temperature Shift
LHHW	Langmuir–Hinshelwood–Hougen–Watson
LTS	Low Temperature Shift
MCFC	Molten Carbonate Fuel Cells
OSR	Oxidative Steam Reforming
PAFC	Phosphoric Acid Fuel Cells
PEMFC	Proton Exchange Membrane Fuel Cell
PFR	Plug Flow Reactor
POX	Partial Oxidation
PROX	Preferential Oxidation
SOFC	Solid Oxide Fuel Cells
SR	Steam Reforming
TOX	Total Oxidation
WGS	Water-Gas Shift

1. INTRODUCTION

In the last century, fast development in industry and increase in living standards led to a drastic increase in total energy demand (Salemme *et al.*, 2010). Though there has been enhancement in efficiency widened spectrum of energy production routes, there is still a direct relation between energy and emission for the conventional energy production technologies. In order to break this relation, technologies alternative to conventional energy production routes have been developed.

The use of Proton Exchange Membrane Fuel Cells (PEMFC) for electricity production on site is one of those alternative technologies to be used in small stationary units, like houses, apartments and small-scale businesses (Holladay *et al.*, 2015).

For PEMFC, hydrogen is preferred due to its high reactivity on the fuel cell electrode and low environmental effect of its product, i.e. water (Löffler *et al.*, 2003). Even though hydrogen is ubiquitous and has too much to offer for producing energy, the biggest drawback is that hydrogen cannot be found freely in nature. Besides, as hydrogen is difficult to store safely and there is no network for its distribution, the use of hydrogen produced as a fuel for energy in distributed units is still impractical. Thus, the hydrogen required for the decentralized energy production by PEMFCs must be supplied on site by fuel processors, which produce hydrogen from hydrocarbons.

Many fuel processor types have been developed recently. The fuel processors models can be distinguished by their fuel types, like methanol, (bio) methane, LPG, etc., and by the way of reforming the fuel (ATR, SR etc.) (Chrenko *et al.*, 2010). A typical fuel processor contains three sequential main units; namely a reformer, a water gas shift and a preferential oxidation unit. (Başar *et al.*, 2016).

The first unit of a fuel processor, reformer, produces hydrogen. Three reactions can be utilized for hydrogen production, namely steam reforming (SR), partial oxidation (POX) and autothermal reforming (ATR) (Löffler *et al.*, 2003). In steam reformer, a hydrocarbon fuel with excessive steam enters the catalytic reactor and generates hydrogen with carbon

oxides. In partial oxidation, oxygen is used to oxidize the fuel to break it into hydrogen, CO, CO_2 and water. An oxidative steam reforming combines the highly endothermic SR and highly exothermic POX reactions to reduce heat demand (Holladay *et al.*, 2015). Autothermal reforming (ATR), however, is a special case when the heat coming from TOX/POX reaction is totally consumed by SR reaction and no further heat treatment is required.

The water gas shift (WGS) process is utilized to reduce the concentration of CO produced in reforming section while producing additional hydrogen (Salemme *et al.*, 2010). In conventional industrial systems, WGS is a two stages unit; the first stage is called high temperature shift (HTS) and operated at 350-420°C whereas the second stage is called low temperature shift (LTS) and operated at 200-220°C. A practical FP impose the design and development of WGS catalysts; having high performance and selectivity towards hydrogen in presence of high H_2 concentration; non-pyrophoric in nature; and enable the use of a single reactor satisfying performance specs in HTS-LTS transition temperatures, Our group have developed several WGS catalysts satisfy those requirements.

CO concentration at WGS outlet, 0.2-1%, is still high for FP-PEMFC operation; therefore, another unit, preferential oxidation (PROX), aiming to reduce the CO concentration at the outlet of FP to or below 100 ppm (Salemme *et al.*, 2010).

A variety of fuels have been considered as feedstock for the fuel processors. These fuels are profoundly the mixture of hydrocarbons with the formula $C_jH_kO_l$. Methane is considered one of the most prominent fuels for fuel processor due to its high availability and its potential for having high efficiencies (Qi *et al.*, 2007). Besides, methane has the highest energy density compared to those of all other hydrocarbons (Holladay *et al.*, 2015).

The current thesis is the part of an ongoing project aiming to design and construct a Demo-scale fuel processor (DFP) that produces sufficient amount of PEM-grade H_2, having CO concentration below 100 ppm, from methane in amount enough to feed a 1 kW PEMFC.

In this context, first of all, the power law type kinetic expressions obtained from kinetic studies for the FP reactions (*OSR, WGS and PROX*) were corrected through

minimizing the difference between experimentally obtained performance test results that had been obtained previously and the results obtained from the mathematical model formed in the current study for the same reaction conditions. In the second part, the fuel processor prototype (FPP) was modeled and its performance was simulated through the use of corrected kinetic models. First FP reactors (OSR-WGS-PROX) having ¼ inch-OD were modeled in series along with their transfer lines. Then, the same simulations were performed for 1 inch-OD of the reactors, which is the OD of the reactors has been planned to be used in Demo-FP. At the final stage of this part, the reaction conditions yielding the best performance in terms of hydrogen production and CO level at the exit of the PROX reactor were selected and for the selected sets of reaction conditions, the simulations performed through the use of DFP model to define the catalyst amounts in the reactors that satisfy the constraints on DFP product, *ie. min.* H_2 *flow and max. CO impurity*, imposed by 1 kW PEMFC. In the last part, the operation of individual OSR reactor was further simulated for granule-size technical catalyst via introducing several levels of effectiveness factor to the power-law type OSR kinetic expression. By using the Fluent based OSR model, the required catalyst amounts and the pressure drop values for the particle diameters and effectiveness factors studied were calculated.

Chapter 2 comprises a comprehensive literature survey including detailed information about decentralized energy production, fuel cells, hydrogen, fuel processors and fluid flow in porous media, followed by technical and experimental information about fuel processor reactions and their modeling. How the calculations and simulations were done is presented in Chapter 3. Chapter 4 includes the simulation results and the related discussions. In the end, Chapter 5 contains the conclusions from the results and recommendations for future work.

2. LITERATURE SURVEY

2.1. Decentralized Energy Production

In contemporary world, electricity is regarded as main driving force of the economic development of all nations, especially for the developing countries. Incessantly producing electricity and meeting the never-ending demand are challenging. In developing countries, more than 50% of the population lives in rural areas (Silva Herran and Nakata, 2012) and establishing infrastructure and supplying electricity to those places becomes more and more unaffordable for governments.

An alternative to electrification of both rural and urban areas is decentralized energy technologies. These technologies discard the strong dependence of onerous centralized energy distribution and allow people to generate electricity cheaper that it would be. In addition, decentralized energy technologies can tap into local energy resources, mostly renewable (Kaundinya *et al.* 2009).

Implementation of decentralized energy systems can also allow countries to remove disparity of energy supply between urban and rural areas. Moreover, since centralized energy systems depend mostly on fossil fuels, it diminishes the emission of environmentally hazardous gases.

2.2. Fuel Cells

Fuel cells are electrochemical devices which convert chemical energy to electrical energy directly. They can run indefinitely as long as hydrogen and oxygen sources are fed to the system. They have two electrodes; anode makes electrochemical oxidation of fuel happen and cathode promotes electrochemical reduction of oxidant (Ramani, 2006). Energy is produced through oxidation of hydrogen to create water (Equation 2.1). The electricity generated from fuel cells vary from few watts to megawatts. It depends on the area of usage.

$$H_2 + \frac{1}{2}O_2 \rightarrow H_2O \tag{2.1}$$

Fuel cells are mostly classified by the choice of electrolyte. There are plenty of fuel cell types, namely; proton exchange membrane fuel cells (PEMFC), direct methanol fuel cells (DMFC), phosphoric acid fuel cells (PAFC), alkaline fuel cells (AFC), solid oxide fuel cells (SOFC), molten carbonate fuel cells (MCFC) (Fuel Cell Today, 2012). Proton exchange membrane fuel cells (PEMFC) are the most compact and lightweight fuel cell type among others. They are easy to utilize, i.e. easy to start and shut down, and have the highest power output density at standard conditions.

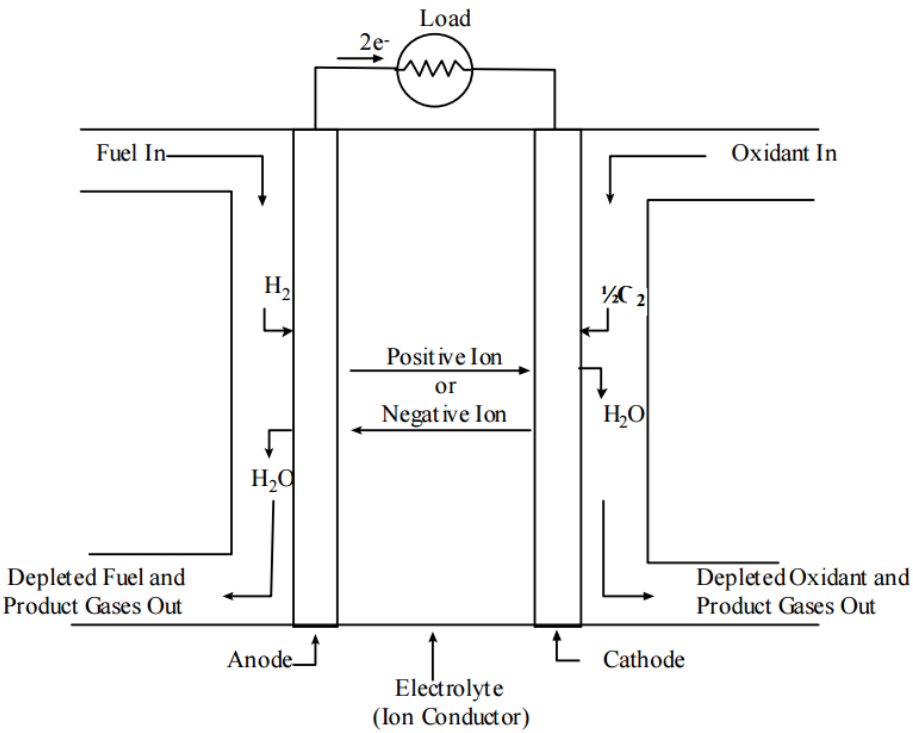

Figure 2.1. Schematic of an individual fuel cell (EG&G Technical Services, Inc., 2004)

2.3. Hydrogen

Air pollution is nowadays one of the biggest threats to the human life. It speeds up the climate change and leads to serious health problems. The main reason for this is the emission of environmentally hazardous gases which are formed during energy production from fossil fuels.

On the other hand, hydrogen energy technologies offer clean energy production. Hydrogen is odorless, colorless, non-poisonous, high in energy and omnipresent; it can be found in virtually all of the organic compounds. The three important features of the energy production from hydrogen in comparison with other technologies are; there is zero emission, the supply is endless and the systems can utilize a variety of energy sources, including renewable (Johnston *et al.*, 2005). The only shortcoming of energy production from hydrogen is that, hydrogen cannot be found freely on earth. It always has tendency to create compounds with other elements. Therefore, in order to extract hydrogen from compounds, a few systems of reactions are required. The most famous and convenient system is called fuel processor.

2.4. Fuel Processors

A fuel processor is where chemical conversion of hydrocarbon to hydrogen gas takes place. A typical fuel processor is lightweight and small, should be placed near the fuel cell. A high conversion rate of hydrocarbon to hydrogen with minimum amount of CO and other toxic compounds designates the quality of the fuel processor. A typical fuel processor should contain two units; a reforming unit and a CO clean-up unit.

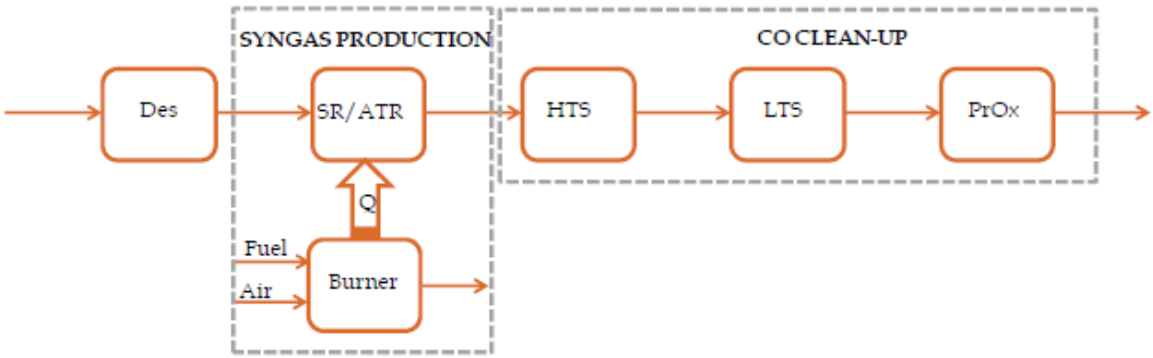

Figure 2.2. Schematic of a simple fuel processor (Salemme *et al.*, 2010)

2.5. Reforming Reactions

Reforming is the main hydrogen production part of the fuel processor. This can be achieved by applying heat to the hydrocarbon feed. There are three types of reforming

processes which can be occur at the reforming stage; steam reforming (SR), partial oxidation (POX) and oxidative steam reforming (OSR) (Löffler *et al.* 2003).

2.5.1. Steam Reforming

Steam reforming is the most common process used in various industries since its selectivity is superior to any other reforming processes. It is achieved by feeding a hydrocarbon fuel and steam to a catalytic reactor, where the following reactions take place:

$$C_mH_{2n} + mH_2O \leftrightarrow mCO + (m+n)H_2 \tag{2.2}$$

$$C_mH_{2n} + 2mH_2O \leftrightarrow mCO_2 + (2m+n)H_2 \tag{2.3}$$

As the reaction goes on, the number of moles present in the reactor will be higher than that of in the feed, therefore the reaction is favored by low pressures. Also, the process is favored by high temperatures, since the reactions are endothermic and additional heat is added to the system. The temperature results in this process does not exceed 800°C due to catalyst deformation (Salemme *et al.*, 2010).

The parameters that affect the process are temperature, pressure and steam to carbon ratio (S/C). The value of S/C should be between 2-4 due to coke formation, high endothermicity and process cost (Avcı *et al.*, 2001).

2.5.2. Partial (POX) and Total (TOX) Oxidation

In both partial and total oxidation reactions, oxygen and the hydrocarbon fuel is mixed to form hydrogen (H_2) and carbon monoxide (CO). These reactions are highly exothermic (total oxidation being much more exothermic than the partial one) and because of it no extra heat is required for these reactions. Reactions are listed below (partial and total, respectively):

$$C_mH_{2n} + (1/2m)O_2 \leftrightarrow mCO + nH_2 \tag{2.4}$$

$$C_mH_{2n} + (m + 1/2n)O_2 \leftrightarrow mCO_2 + nH_2O \quad (2.5)$$

POX reaction is a very fast reaction. It uses very low O_2/fuel ratio. The reaction rate of POX is much more than that of SR. The reaction can occur without a catalyst, but if an appropriate catalyst is used, the maximum temperature will drop drastically. The non-catalytic process operates at 1100-1500 °C, whereas the catalytic one at 600-900 °C.

Even though POX is faster than SR, it has some disadvantages. Due to lower hydrogen production and higher coke formation, SR is favorable (Shekhawat *et al.*, 2011).

2.5.3. Oxidative Steam (OSR) and Autothermal (ATR) Reforming

Oxidative steam reforming (OSR) is the combination of the steam reforming and partial oxidation. It combines the endothermicity of steam reforming and exothermicity of partial oxidation to minimize the heat requirement and to maximize the hydrogen production. Through this, higher concentration and lower coke formation can be achieved. The reactor sizes are smaller than the reactor size of a POX reaction. Hydrogen production rate can be increased by changing steam to oxygen (H_2O/O_2) ratio (Salemme *et al.*, 2010).

OSR reaction is not simply combination of steam reforming and partial oxidation, there are many reactions take place simultaneously. Some of them are desired reactions which result in increase in H_2 concentration in the outlet stream such as TOX and WGS.

In contrast with the desired reactions, some undesired reactions can occur within the reactor. These reactions are methanations (Equation 2.6 and 2.7), reverse water-gas shift (Equation 2.8), hydrogen oxidation (Equation 2.9), Boudouard reaction (Equation 2.10) and hydrocarbon decomposition (Equation 2.11) (Shekhawat *et al.*, 2011).

$$CO + 3H_2 \leftrightarrow CH_4 + H_2O \quad (2.6)$$

$$CO_2 + 4H_2 \leftrightarrow CH_4 + 2H_2O \quad (2.7)$$

$$CO_2 + H_2 \leftrightarrow CO + H_2O \tag{2.8}$$

$$H_2 + 1/2O_2 \leftrightarrow H_2O \tag{2.9}$$

$$2CO + CO_2 \leftrightarrow C \tag{2.10}$$

$$CH_4 \leftrightarrow C + 2H_2 \tag{2.11}$$

Başar *et al.* investigated the steady state reaction of OSR reactor. OSR of methane was conducted over novel Pt-Ni/δ-Al_2O_3. The temperatures were 623, 673, 723 and 773 K and S/C ratios were 2.25, 3, 5 and 6 in the OSR feed (respective W/F ratios were 1.68, 1.5, 1.19 and 1.07 mgcat min μmol^{-1}). Simultaneous use of high temperature and high S/C ratio led to increased H_2 and H_2/CO ratios, and decreased CH_4 and CO_2 concentrations in OSR product. Maximum achieved methane conversions at 623, 673, 723 and 773 K were 45%, 56%, 69% and 94%, respectively. Oxygen fed to the OSR was totally consumed in all tests. OSR temperature of 723 K, S/C ratio of 5 in the OSR feed were the optimal parameters targeting high H_2/CO product ratio. The experimental product distribution trends were highly consistent with the results of the calculations of thermodynamic equilibrium.

In the study of Erdinç (2014), the aim was to obtain a power law type rate expression for methane OSR over Pt-Ni/δ-Al_2O_3. Based on the outcomes of the performance test results, the kinetic study was performed at 375 °C with carbon to oxygen feed ratio between 4 and 7.34 and steam to carbon feed ratio between 2.03 and 3.08. 17 pairs of kinetic experiments were conducted by changing inlet compositions of reactants (methane, oxygen, and steam) and residence time (W/F). Reaction orders were estimated as 0.81, 1.60 and 0.44 for methane, oxygen and steam, respectively, by using multivariable non-linear optimization function of MATLAB. The apparent activation energy and pre-exponential factor were calculated as 31.99 kJ mol^{-1} and 0.366 μmol $mgcat^{-1}$ s^{-1} $kPa^{-2.85}$ for the temperature range 350-425 °C.

2.6. Water Gas Shift (WGS) Reaction

The water gas shift reaction (WGS) is a reaction which produced H_2 from synthesis gas. It is mostly used after hydrocarbon steam reforming to reduce CO level and increase H_2 production at the same time. The WGS reaction is a moderately exothermic reversible reaction and thermodynamically limited at high temperatures (Smith *et al.*, 2010).

$$CO + H_2O \leftrightarrow CO_2 + H_2 \tag{2.12}$$

As the temperature increases, the equilibrium constant of reaction decreases. Therefore, it can be said that the reaction is thermodynamically favored at low temperatures and kinetically favored at high temperatures. Through the reaction, no change in total mole can be observed since the sum of stoichiometric coefficients of reactants is equal to the sum of stoichiometric coefficients of products. Thus, the reaction is not affected by pressure. The catalyst used for WGS reaction can be metals or metal oxides.

The WGS reactor are generally designed as adiabatic reactors, in which temperature increases through the catalyst bed, due to the exothermic nature of the reaction. The WGS reactor has two stages. The first stage is called high temperature shift reaction (HTS) and generally operates at 320-450 °C using Fe-Cr oxide catalysts. The last stage is called low temperature shift reaction (LTS) and generally operates at 200-250 °C using $Cu/ZnO/Al_2O_3$ or precious metal-based catalysts (Maklavany *et al.*, 2016; Natesakhawat *et al.*, 2006).

Kesim (2017) investigated the performance of Pt-based, CeO_2 supported trimetallic Pt-Re-V/CeO_2 catalysts having high activity, selectivity and stability with suppressed methanation in WGS reaction. Performance tests were conducted under realistic feed composition, at 300, 350 and 400 °C with fixed W/F as 0.5 mgcat min ml^{-1}. In the study, catalyst composition, temperature and H_2O/CO ratio in the feed were used as parameters of experiments. The results showed that, 1Pt-0.5Re-1V/CeO_2 and 1Pt-0.5Re-0.5V/CeO_2 have huge potentials to be used in WGS reaction as catalyst owing to their high activity, stability and selectivity. Another important point is that, those catalysts can make a single stage WGS unit possible instead of conventional two stages (HTS and LTS) WGS unit in a fuel processor.

In the study of Yumru (2017), the aim is to obtain a power law type kinetic expression for a WGS reaction over 1Pt-0.5Re-1V/CeO_2 catalyst under realistic feed conditions. In this content, the preliminary kinetic tests were conducted to determine kinetically controlled and mass transfer limitations free experimental conditions. The kinetic experiments were conducted with S/C feed ratio ranging from 15 to 45 at 350 °C and 1 bar. 17 pairs of kinetic experiments were performed by inlet compositions of CO, H_2O, H_2, CO_2 and CH_4, and residence time, W/F. Data from experiment results were used to estimate kinetic parameters of the power-law kinetic model by using the method of initial rates and non-linear regression analysis in MATLAB. The reaction orders of CO, H_2O, H_2, CO_2 were estimated as 0.82, 0.31, -0.29 and -0.35 within $\pm$6% error, respectively. In addition, the effect of methane in WGS feed was investigated, and the kinetic reaction rate was found to have no dependance on the concentration of CH_4 in the feed stream. In addition, β' values were obtained in the range of 0.054–0.163. The apparent activation energy and the frequency factor were found to be 25.65 kJ mol^{-1} and 18.09 μmol $mgcat^{-1}$ s^{-1} $kPa^{-0.49}$, respectively.

2.7. Preferential Oxidation (PROX) Reaction

The preferential oxidation is a reaction in which carbon monoxide is converted into carbon dioxide in the presence of oxygen. It is industrially used to remove or sharply decrease the CO level of a mixture. It is most commonly used in fuel processor reactions to reduce the CO mole fraction from 1-2% to below 100 ppm.

For an energy efficient fuel processor, the temperature of PROX reaction should be between the operating temperature of fuel cell (80-100 °C) and that of low temperature WGS reaction (200-250 °C) (Mariño *et al.*, 2004). Even though the most convenient temperature for PROX reaction is 100-130 °C, high temperatures are required for preventing irreversible CO adsorption.

Low temperature CO oxidation with a catalyst has two main reaction steps, which occurs simultaneously. First CO chemisorption occurs and then dissociative adsorption of O_2 follows. Thus, to minimize the problems result from adsorption competition, the catalyst must have different active sites for each of the reactants and/or chemisorption processes in order to have high activity and stability (Çağlayan *et al.*, 2011). The catalyst type used for

this reaction is mostly noble metal catalysts (Pt, Ir, Pd), most notable oxide-supported types. In addition, H_2 oxidation may occur as an undesired reaction in small amount.

$$CO + O_2 \leftrightarrow CO_2 \tag{2.13}$$

Çağlayan *et al.* (2011) studied preferential CO oxidation over 1% Pt–0.25% Sn supported on nitric acid (HNO_3) treated with activated carbon (AC-N) for various feed compositions. The performance of the PROX catalyst and the effect of reaction parameters on activity and selectivity were investigated. Factors resulting in high performance of the Pt–Sn/AC-N catalyst were scrutinized by O_2 and CO adsorption and PROX tests conducted on an in situ diffuse reflectance IR Fourier transform spectroscopy system followed by a mass spectrometer. The results showed that the presence of CO_2 and H_2O in the feed does not significantly affect the CO conversion and selectivity of the catalyst. In all tests, CO conversion increased with the decrease in temperature within 135-110 °C range, indicating enhancement in CO selectivity as the temperature decreases. The CO conversions of the catalyst for the H_2 rich feed including CO_2, H_2O and CH_4 were in the range of 75%-90% at 110 °C.

In the study of Eropak and Aksoylu (2017), a kinetic study of preferential CO oxidation in the presence of H_2, CO_2, H_2O, and CH_4 over 1% Pt–0.25% Sn catalyst supported on nitric acid (HNO_3) treated with activated carbon (AC-N) prepared by the sequential impregnation method. The kinetic experiments were conducted at 110 °C and 1 bar, and different sets of CO and O_2 concentrations, each with different space times and catalyst loadings, were used. Molar concentrations in the feed were varied between 1-2.5% CO and 1-1.5% O_2. The experimental data used to estimate kinetic parameters of the power-law kinetic was modeled by using the method of initial rates. Reaction orders with respect to CO and O_2 were found as 0.47 and -0.57 at 110 °C. The apparent activation energy and the frequency factor were found to be 45.300 kJ mol^{-1} and 5.83×10^7 μmol mg^{-1} min^{-1} $kPa^{0.1}$, respectively. The variance of experimental error was found to be ±0.1019 (μmol mg^{-1} min^{-1})^2 for this rate expression, which points out that experimentally measured and model predicted rates was not perfectly fitted due to the presence of a secondary mechanism through water activation involving surface OH^- group.

2.8. Fluid Flow in Porous Media

A porous medium consists of particles and pores between particles in a control volume. The existence of particles in the bed reduces the volume available for fluids to flow through. Therefore, in order to maintain the continuity, velocity within the bed should be bigger than it would be when there was no porous medium. The resistance to flow is proportional to the number of particles. When there is no particle in a control volume, the resistance becomes zero. On the other hand, when the control volume is full of particle and there is no space between each other, the resistance becomes infinite. The resistance to flow induces pressure drop within the flowing fluid.

2.8.1. Reynolds Number and Flow Regimes

In a porous medium, energy loss occurs due to viscous drag. As the viscous drag increases, the loss increases. If this viscous drag is low, flow is called laminar flow. When this viscous drag is high due to eddies formed in the porous medium, it is called turbulent flow. Reynolds number (Re) is a unitless number which indicates flow regime of the fluid. If the Re number exceeds 2000, the flow is accepted as turbulent flow, if not, it is called laminar flow.

$$Re = \frac{\rho\, u\, d}{\mu} \tag{2.14}$$

Where;

P = density of the fluid (kg/m^3)

u = flow rate of the fluid (m/s)

d = characteristic length (m)

μ = dynamic viscosity (Ns/m^2)

Characteristic length can also be defined as;

$$d = \frac{\varepsilon}{(1-\varepsilon)S_v} \tag{2.15}$$

Where;

ε = porosity

S_v = specific surface exposed to the fluid (m^{-1})

S_v is defined as;

$$S_v = \frac{S_p}{V_P} \tag{2.16}$$

With the assumption that, the particles are all spherical, S_v becomes;

$$S_v = \frac{\pi\, d_p^2}{\pi\, d_p^3/6} = \frac{6}{d_p} \tag{2.17}$$

Where;

S_p = Surface area of particle

V_p = Volume of particle

d_p = Particle diameter

Combining Equation 2.14 and 2.15 yields modified Reynolds number;

$$Re = \frac{\rho\, u\, \varepsilon\, d_p}{6\, \mu\, (1 - \varepsilon)} \tag{2.18}$$

2.8.2. Porosity

Porosity is the most important parameter of a porous medium. Porosity depends on particle properties, bed properties and packing method. Porosity can simply be defined as the ratio of the porous volume to the total volume of the bed. According to Leva (1951) 1% decrease in the porosity produced about 8% increase in the pressure drop, whilst Carman (1938) found that 1% decrease in the porosity produced 10% increase in the pressure drop. Incompressible glass beads like marbles have around 45% porosity, whereas alumina

particles reach 75% porosity and even biological materials such as yeast cell can reach up to 90% porosity (Abbas, 2011).

The exact porosity value can be calculated experimentally (Pushnov, 2006);

$$\varepsilon = 1 - \frac{\rho_b}{\rho_s} \tag{2.19}$$

Where;

ρ_b = Bulk density of the catalyst (kg/m^3)

ρ_s = Solid density of the catalyst (kg/m^3)

It is also suggested that, porosity value can be calculated and formulized from particle diameter (d_p) and reactor diameter (D_r);

$$\varepsilon = \frac{A}{(D_r/d_p)^n} + B \tag{2.20}$$

Up to day, many equations proposed for finding porosity from d_p and D_r (Furnas, 1931; Feng and Yu, 1998; Pushnov, 2006).

2.8.3. Permeability

The permeability (k) is the measure of the flow conductance of the porous medium. It is defined by the Darcy's law (Mota *et al.*, 1999);

$$k = \left(\frac{\varepsilon}{\tau}\right)^2 \frac{\varepsilon\, d_p^2}{36\,(1-\varepsilon)^2\, K_c} \tag{2.21}$$

Where;

τ = Tortuosity

K_c = Kozeny constant

Kozeny derived a permeability equation related to porosity;

$$k = c \frac{\varepsilon^3}{S_v^2 \tau} \tag{2.22}$$

Carman set the constant c to 1/5 and the Kozeny-Carman equation becomes;

$$k = \frac{d_p^2 \varepsilon^3}{180 (1-\varepsilon)^2} \tag{2.23}$$

2.8.4. Inertial Resistance

Inertia is the resistance in a flow to change its state of motion. In a flow through porous body, there are some losses due to expansion and constriction in the pore channels. The energy loss due to inertial resistance is called inertial loss. Since it is proportional to the square of the velocity, at low velocities (in laminar flow), it has virtually no effect in comparison to the viscous effect. However, in turbulent flows, inertial resistance exceeds the viscous resistances (Idel'chik, 1960).

2.8.5. Ergun Equation

As a fluid flows through a porous body, it experiences a decrease in pressure due to friction in order to maintain its velocity. Relationship between pressure drop and velocity was suggested by Darcy (1896) and Carman and Kozeny (1937). These applications were only valid for laminar flows, in other words, only when the velocity is low, the Carman-Kozeny equation is valid. As the velocity increases, flow becomes turbulent and it tries to retain its initial state and that causes an inertial resistance.

Ergun (1952) presented a general equation for both laminar and turbulent flows. In a randomly packed bed, the pressure drop becomes;

$$\frac{\Delta P}{L} = \frac{150\, \mu\, u\, (1-\varepsilon)^2}{d_p^2\, \varepsilon^3} + \frac{1.75\, \rho\, u^2 (1-\varepsilon)}{d_p\, \varepsilon^3} \tag{2.24}$$

2.8.6. Effectiveness Factor

Pressure drop is one of the prime concerns in the study of fluid flow through a porous body. For an ideal flow, the pressure drop is expected to be low enough to give rise to unexpected problems.

In laboratory scale experiments, powder catalysts are used. Powder catalyst is a type of catalyst which contains particles with very small particle diameters (mostly in μm) and has low porosity. From Ergun equation (1952), it can be clearly seen that, as the particle size increases, pressure drop decreases. In laboratory scale production, this pressure drop can be negligible, but in industrial scale, production rates are far more than that of lab scale. In order to achieve this, more catalyst should be used and this causes increase in catalyst bed length which induces to a very high pressure drop. To prevent this, particle diameter of catalysts can be increased accordingly.

In powder catalysts, there is nearly no diffusional resistance. If the diffusion is fast, the concentration in the pellet would be equal to the concentration of surface everywhere. As the particle size increases, intraparticular mass transfer is limited due to diffusional resistance and the diffusion becomes slower.

The effectiveness factor is commonly used to take the interaction between pore diffusion and reaction into account. The effectiveness factor is defined as; the ratio of the actual reaction rate observed to the reaction rate calculated if the surface reactant concentration persisted throughout the interior of the particle (Hong *et al.*, 1999).

$$\eta = \frac{actual\ rate\ of\ reaction}{rate\ of\ reaction\ without\ diffusional\ resistance} \tag{2.25}$$

The effectiveness factor is a unitless pellet production rate which shows how effectively the catalyst is used. As η goes to 1, since the reactant is able to diffuse quickly through the pellets, the entire volume is reacting at the same high rate. As η goes to 0, the pellet reacts at a low rate, because the reactant is unable to penetrate into the interior of the

pellet. The diffusional resistance of the pellet is large and this lowers the overall reaction rate (Rawlings and Ekerdt, 2015).

2.9. Modeling of Fuel Processor Reactions

Barrio *et al.* (2006) investigated catalytic partial oxidation with steam reforming. One-dimensional quasi homogeneous reactor model was selected for ATR reactor. A fixed-bed reactor was used. The catalyst was chosen to be the 5% Ru supported on γ-Al_2O_3. The temperature was between 873 and 923 K at 3.1 bars. The partial oxidation was carried out on a combination of combustion and steam reforming. In the reactor, a number of reactions occur, however only four of them were taken into account since some of them are the combination of others and some of them do not have significant rates. The reactions took place were; exothermic combustion, endothermic steam reaction to CO, endothermic steam reaction to CO_2 and water gas shift reaction.

For these reactions, the rate equation suggested by Ma *et al.* (1996) and Xu and Froment (1989), which are based on Langmuir–Hinshelwood model. For the first reaction, data for Pt-based catalyst; for the other reactions, data for Ni-based catalyst were taken from the literature. Data from the literature with different feed compositions and molar ratios were compared with the results of the simulation. The activation energy and the pre-exponential factors for Ru-based catalyst were matched well with Ni and Pt-based catalysts. The outlet flow rates were fitted well with deviation less than 18%. Moreover, the formation of the hot spots was also analyzed.

The main scope of the paper written by Zahedi *et al.* (2009) was to propose a mathematical modeling for ATR having two sections, the first part being combustion section and the second part being catalytic bed section. The catalyst used in the second part was Ni/Mg-Al_2O_4, whereas the first part required no catalyst. In order to model the system, multi-dimensional continuous stirred tank reactor (CSTR) and batch adiabatic reactor models were utilized.

The simulation of the first part consists of 108 single step elementary reactions in which 28 species are involved in adiabatic conditions. For the second part of the system, the

temperature profiles, catalyst surface and the gas composition were predicted with a heterogeneous catalytic reaction model. The reactor was considered as a cylinder filled with catalyst. In this part, only the reactions with significant rates were considered. The reactions are endothermic steam reforming to CO, endothermic steam reforming to CO_2 and water gas shift reaction. Their respective kinetic rate equations were taken from the literature (Xu and Froment, 1989) and multiplied with different effectiveness factors.

Mass and energy balance equations were also taken into account when simulating the whole system. The temperature required for the system to guarantee the highest conversion is 1700 K. As the temperature increased, rate of reaction increased and time required for reaching equilibrium decreased. The results of the mathematical modeling were in good agreement with the data available in literature.

In the study of Akbari *et al.* (2011), autothermal reforming of methane was simulated in a rectangular surface reactor using a three-dimensional computational fluid dynamics (CFD) model. The governing equations in the model consisted of mass, energy, chemical species and momentum. To achieve this, the model was homogeneous and three-dimensional. Four reactions were occurred in their system in gas-phase over Ni/Al_2O_3 catalyst in a temperature range of 400-600 °C; the exothermic total combustion of CH_4, the endothermic steam reforming of CH_4 to CO, the water gas shift reaction and the steam reforming of methane directly to CO_2 (Trimm and Lam, 1980; Xu and Froment, 1989; Ma *et al.*, 1996).

On the microreactor walls, surface reactions occurred. For these reactions, the rates of formation and consumption were calculated by summing up the reaction rates of every species in all the reactions. In addition, effectiveness factor for all reactions were added to the reaction rates to correct the rates. On the other hand, within the reactor, a gas-phase methane oxidation took place and for this, a global mechanism suggested by Westbrook and Dryer (1981) was considered. Moreover, Navier-Stokes equation, mass and energy balance equations were added to the model and the finite volume method was established to solve the non-linear equations.

The optimum conditions were observed as; feed temperature: 600 °C, space velocity: 50,000 h^{-1}, A/F: 1.0 and W/F: 3.0. At those conditions (dry basis); H_2 and CO mole fractions were found to be 38.9% and 4.8%, respectively.

In the paper written by Lattner and Harold (2005) three systems were compared. All systems used methanol as feedstock and produced hydrogen as product. The way they produced hydrogen was slightly different from each other. The first one used SR with PROX, the second one used ATR with PROX and the third one only used ATR Pd membrane. $CuO/ZnO/Al_2O_3$ catalyst was utilized for oxidation and reforming reactions. In steam reforming section, steam reforming of methanol, decomposition of methanol and water gas shift reaction took place. In addition, for the ATR reaction, oxidation of methanol was also observed. For those reactions, the kinetic models proposed by Peppley *et al.* (1999) and Reitz *et al.* (2000) were taken into account.

In addition to the rate equations, mass and energy balance equations were conducted in the simulation. Moreover, hydrogen permeability of the membrane was calculated. Finally, effectiveness factor was added to the reaction rate and effectiveness factor was found to be highly dependent of temperature.

The results of the simulation had a good agreement with the results present in literature. In the end, it was concluded that, although the adiabatic ATR Pd membrane reactor can deliver purer H_2 relative to the others, the efficiency of the ATR Pd membrane system was less than the other systems due to the fact that excess amount of steam was required for the ATR Pd membrane reactor system.

Choi and Stenger (2003) studied the kinetics of the WGS system. The reactions were carried out at 120-150 °C and over $Cu/ZnO/Al_2O_3$ catalyst. The system was assumed to be one-dimensional isothermal plug-flow reactor PFR model. WGS system has two sub-steps inside. In the first step water adsorbs and dissociates on reduced sites of catalyst surface to produce hydrogen while oxidizing a site. In the following step CO is oxidized to CO_2 on this oxidized site. From these two mechanics, five rate expressions were acquired (Froment and Bischoff, 1990; Newsome, 1980; Keiski *et al.*, 1993). In order to select the most appropriate model, data from literature were gathered and checked if the data fit the rate expression by

using non-linear least squares optimization. Among them, the double site Lanmuir-Hinshelwood type rate expression from the adsorptive mechanism and the single path redox mechanism were selected. To maintain a constant flow rate of CO and H_2O, temperature and water addition rate should be observed with care.

Lin *et al.* (2005) proposed an experiment for methane fuel processor operated in three stages; heat-up, autothermal reforming, steam reforming. A one-dimensional, homogeneous PFR was assumed for the heat and material balances. Steam reformer, water gas shift and preferential oxidation were used simultaneously in this system and their rate expressions were found in literature.

In ATR, three reactions took place; the endothermic steam reforming of CH_4 to CO, the exothermic water gas shift and the endothermic total oxidation of CH_4. The catalyst was Ru/CeO2-ZrO2 catalyst. The rate expressions taken from the literature were the ones suggested by Xu and Froment (1989) and Trimm *et al.* (1980). In WGS reactor, the rate expression proposed by Choi and Stenger (2003) and in PROX reactor, the rate expression proposed by Amphlett *et al.* (1996) were used to model the reactors. In addition, two high-temperature WGS reactors (HTS1 and HTS2) and one low-temperature WGS reactor (LTS) were utilized in the WGS reactor.

Since the reactor temperatures are different within the system, heat exchanger and cooling units were also added and energy balance was conducted accordingly. The pre-exponential factors of the rate constants were adjusted to fit the experimental data and the result provides a well description of steady-state behavior.

The ATR reactor yielded a H_2 yield of 1.28 moles min^{-1}, a CO concentration of 40 ppm and 66% efficiency. On the other hand, the SR reactor gave a H_2 yield of 1.18 moles min^{-1}, a CO concentration of 30 ppm and 51% efficiency. The ATR reaction resulted in higher efficiency and larger hydrogen yield with lower inlet temperature than the SR reaction. Therefore, the ATR reaction should be the reaction of choose. These H_2 productions corresponded to a power generation of 2 kW.

Lin *et al.* (2006) developed a dynamic model for a series for reaction which produces hydrogen from methane. The reactions are in series starting from reforming (ATR), high and low water gas shift reactions (HTS/LTS) and preferential oxidation (PROX). In this paper, fuel processor system was fully established including heat exchangers. The system was modeled with the assumption homogeneous one-dimensional plug-flow reactor (PFR) model for simplicity. The pressure was constant. Energy and mass balances for the system were also added to the model.

Two distinct control systems were implemented to the system to keep the CO level below 100 ppm. One utilized the inlet flow rate as the throughput manipulator, which was called on-supply structure and the other one utilized the outlet flow as the throughput manipulator, which was called the on-demand structure. The results showed that, on-demand structure gave faster responses to the system.

Pacheco *et al.* (2003) developed a mathematical model for reforming of isooctane. ATR was utilized and in order to reduce the concentration of CO, WGS system was also added to the system. Aspen Plus process simulator was used for the calculations of the mathematical models. The reaction kinetics for both systems were taken from the literature and modeled using Langmuir–Hinshelwood–Hougen–Watson (LHHW) formulation to take the adsorption effect into account. The catalyst for the first part was Pt-CeO_2. Even though the kinetic data for the systems prepared with this specific catalyst were too scarce, kinetic data for other catalytic systems were taken from Jin *et al.* (2000), Xu *et al.* (1989) and Rostrup-Nielsen (1984) and regressed according to the system on this paper. In addition, effectiveness factors for each reaction were estimated.

Due to the high temperature, diffusional limitations and heat transfer played important roles in the reactor performance and because of them, heat and mass transfer equations were also included. The model predicted the available experimental data for the distribution of H_2, CO and CO_2 in reformate with a deviation of about 15%.

3. CALCULATIONS

In this study, all the results obtained from the experimental data were the output of ANSYS Fluent. ANSYS is an engineering simulation software which allows its users to solve challenging product engineering problems. Fluent is a module of ANSYS specialized for fluid flow in a vessel. One of the prime advantages of using Fluent is to model the fluid flow in 3-D. It also enables its users to take reaction into account. The main advantage of this program is to be able to simulate a flow in a porous media which allows Fluent to distinguish itself from other calculation softwares such as MATLAB and Polymath.

Polymath calculations of the experimental test results were also presented in this study, in order to illustrate the distinction between flow in porous and non-porous media. In addition, MATLAB was used in order to take the inverse of 5x5 matrix and to calculate the molar flow rate of H_2O in outlet in calculation of OSR system in later sections.

3.1. ANSYS Fluent Simulations

3.1.1. Creating the Geometry

In the first part of simulating the demo-scale fuel processor system, creating the geometry of the OSR, WGS and PROX systems separately. The configurations were based on the specifications of the reactors used in experimental setup. The specifications are given in Table 3.1.

Table 3.1. Specifications of reactor used in experiments

Parameter	Value (cm)
Outer diameter	0.64
Inner diameter	0.46
Total length of reactor	37
Length of catalyst bed	0.4 - 3

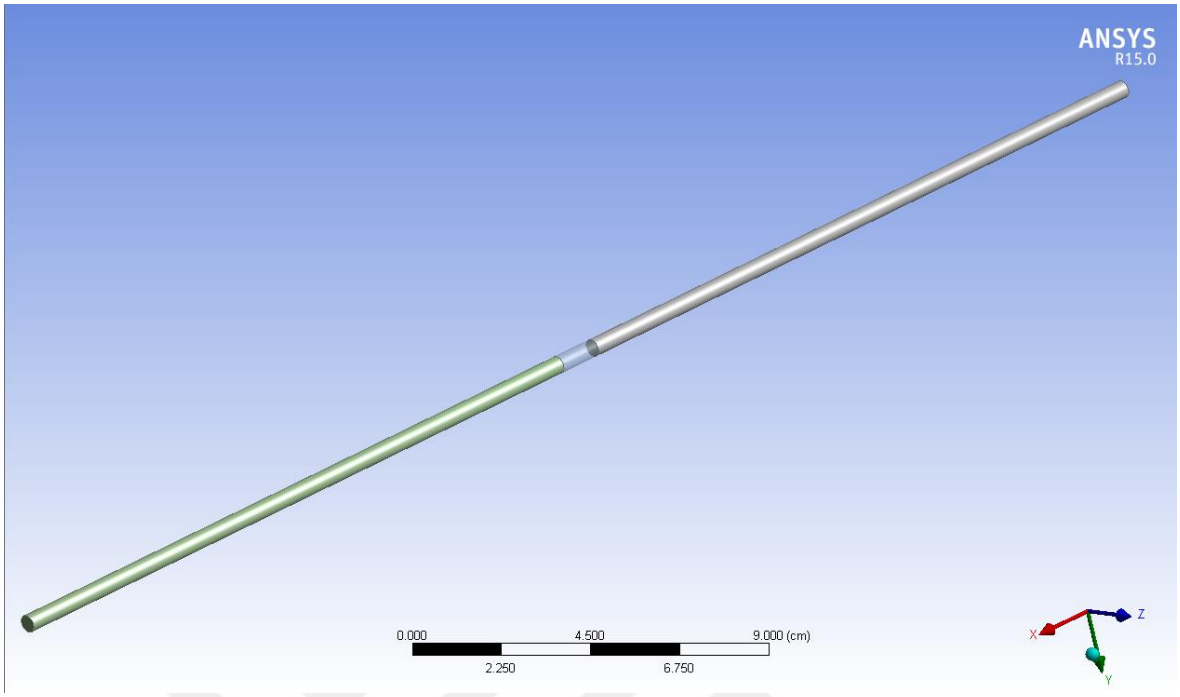

Figure 3.1. Modeled geometry of a reactor

The tubes used in the experimental setup have an outer diameter of 0.25 inches but tubes having 1 inch also modeled for creating a system which produces sufficient amount of H_2 for 1 kW PEMFC keeping residence time (W/F) constant. The catalyst bed was fixed at the center of the reactor (Figure 3.1). The length of the catalyst bed varies with the catalyst amount and density of the catalyst. Calculated density values are shown in Table 3.2 for OSR, WGS and PROX catalysts.

Table 3.2. Densities of catalyst used in FP reactions

Reaction	**Catalyst**	**Density (g/cm^3)**
OSR	0.2Pt-10Ni/δ-Al_2O_3	0.77
WGS	1Pt-0.5Re-1V/CeO_2	0.93
PROX	1Pt-0.25Sn/AC	0.44

For the second part of the calculations, three reactions were combined consecutively with the assumption of pipes having 1 cm length were used to connect the reactors. In addition, at the beginning of the PROX reactor, additional O_2 supply line was implemented,

because in OSR reactor, all the O_2 that were supplied to the system were totally depleted and there was no O_2 to react with CO in the PROX reactor (Figure 3.2). Moreover, in case of backflow, the O_2 supply line was implemented having 45° with respect to the reactor and a mixing area was also added between WGS and PROX reactors.

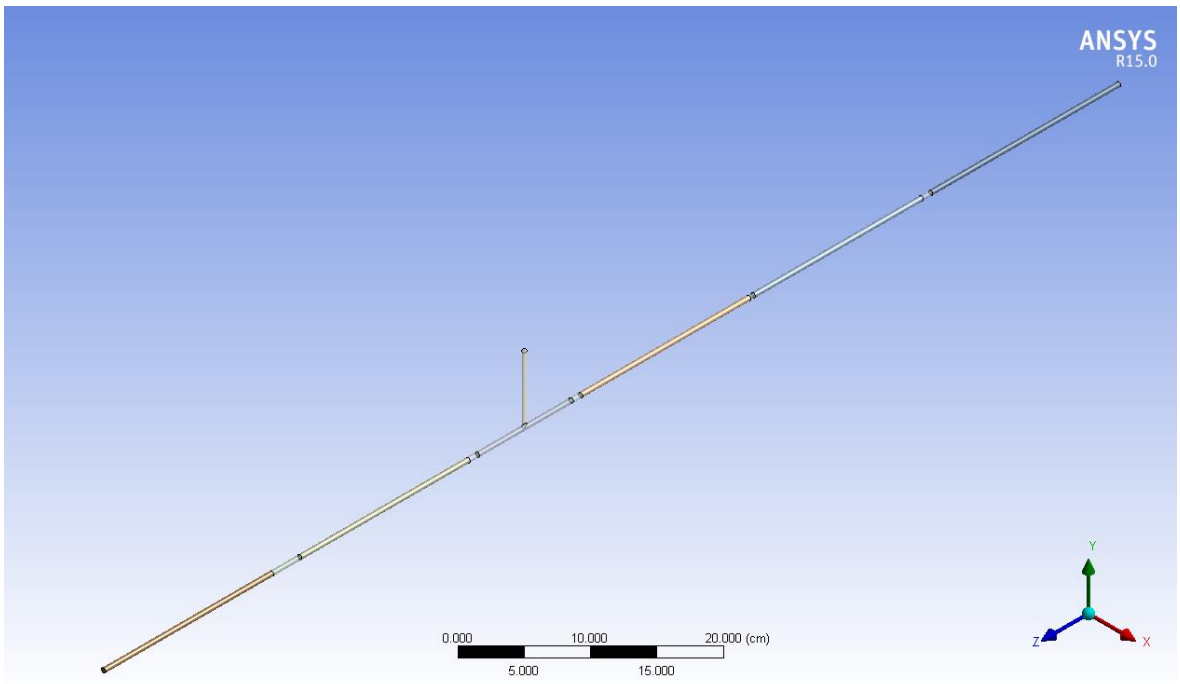

Figure 3.2. Modeled geometry of a fuel processor unit

3.1.2. Meshing the Geometry

In ANSYS Fluent, meshing the geometry is one of the most important aspects of the simulation. By meshing the geometry, cells were created in many points of the geometry and Fluent solves the governing equations from node to node. As the number of cells increases, the system gives more accurate results. On the other hand, the time for solving the system increases accordingly. In order to have the perfect meshing, the cell sizes are determined in a way that, the errors emanated from bigger cell size should be insignificant and the time loss emanated from having too many cells should not be too much.

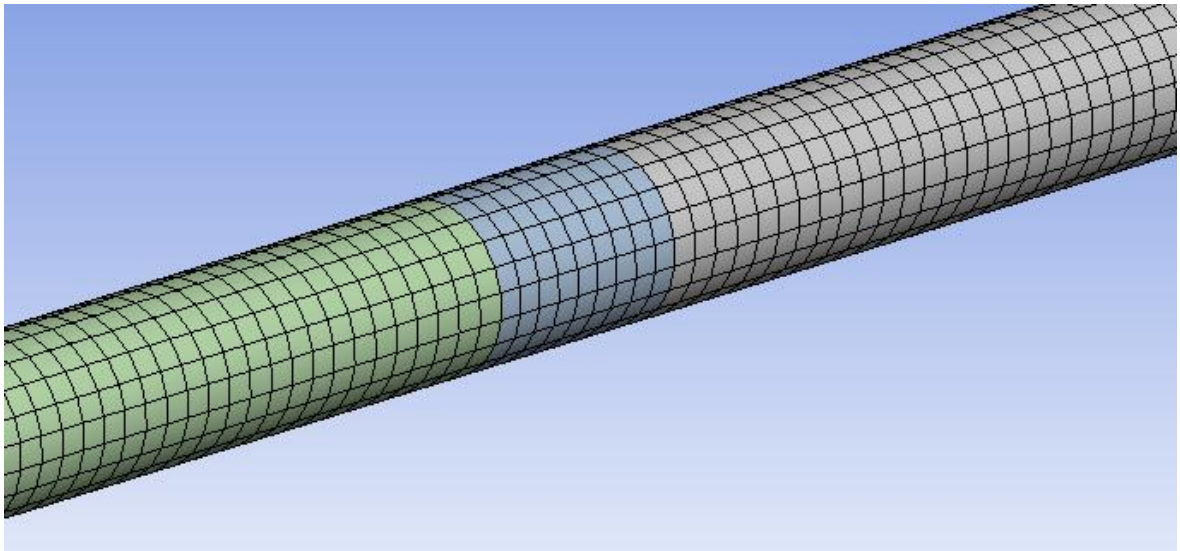

Figure 3.3. Cells created by ANSYS Meshing

3.1.3. Fluent

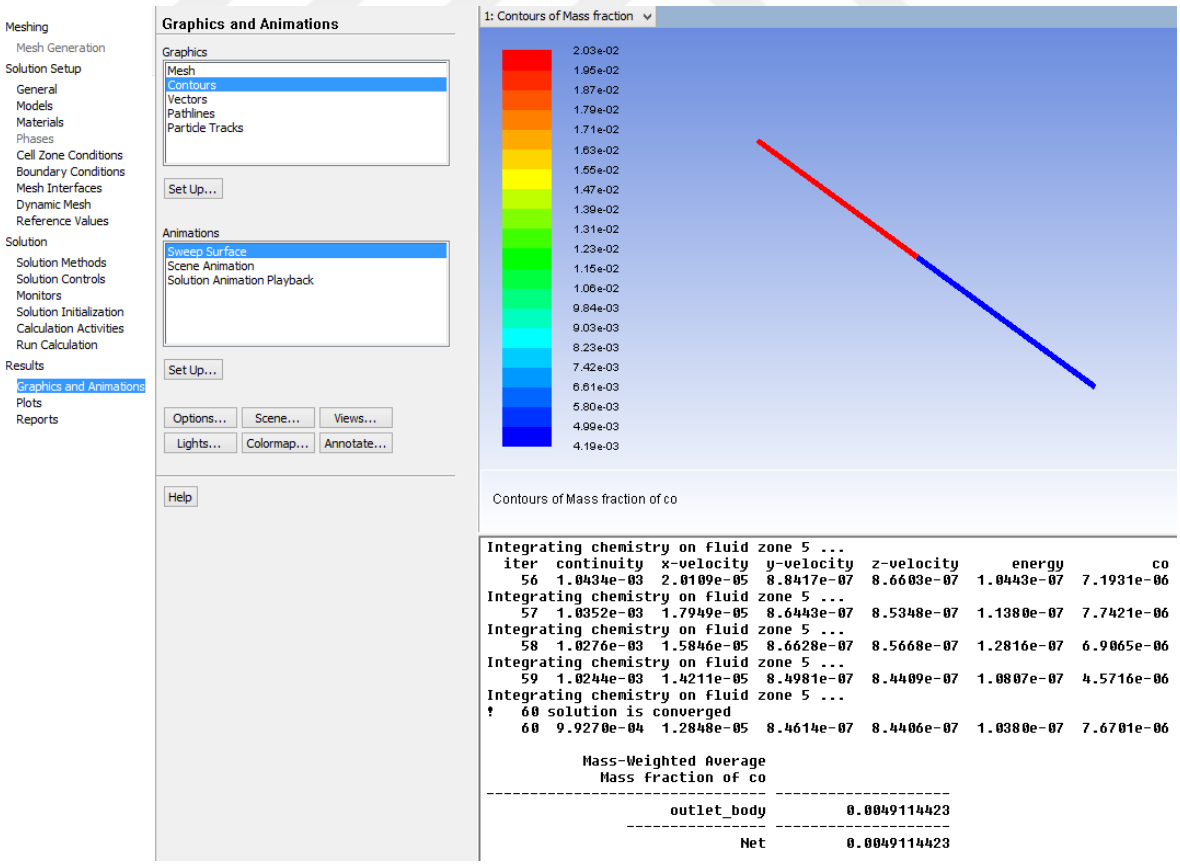

Figure 3.4 ANSYS Fluent

ANSYS Fluent is where the calculations are made. The parameters which are determined by user, are;

- Species used in reactions
- Flow type
- Reaction type
- Number of reactions
- Reaction mechanisms
- Stoichiometric coefficient of species in reactions
- Rate exponent of species in reactions
- Pre-exponential factor (kmol /m^3 s)
- Activation energy (j/kmol)
- Viscous resistance (1/permeability) (1/m^2)
- Inertial resistance (1/m)
- Porosity (%)
- Reaction temperature
- Inlet velocity magnitude (m/s)
- Inlet temperature (K)
- Inlet pressure (bar)
- Inlet species in mole fractions

After specifying every parameter, Fluent can calculate the solution.

3.2. Polymath Calculations

Before evaluating the experimental data in ANSYS Fluent, Polymath is utilized in order to check the correctness of the parameters will be used in Fluent. The power-law type rate expression and the differential form of the packed bed reactor design equation are written (Equation 3.2 and 3.3) for a simple one-step reaction;

$$A + B \rightarrow C + D \tag{3.1}$$

$$-r_A = \left[k_0 e^{\left(\frac{-E_A}{RT}\right)}\right] P_A^{\alpha} P_B^{\beta} P_C^{\gamma} P_D^{\delta} \tag{3.2}$$

$$-r_A = \frac{dF_A}{dW} = F_{0_A} \frac{dX_A}{dW} \tag{3.3}$$

For Polymath, in the first power-law type rate expression, partial pressures can be replaced by concentration values but it is not mandatory. In contrast, Fluent only accepts concentration values in the rate expression. Therefore, for simplicity, partial pressure values are converted into concentration values in both Polymath and Fluent calculations by ideal gas law (Equation 3.4 and 3.5), and then the combination of Equation 3.2 and 3.3 yields the differential equation;

$$PV = nRT \tag{3.4}$$

$$P = CRT \tag{3.5}$$

$$\frac{dX_A}{dW} = \frac{\left[k_0 e^{\left(\frac{-E_A}{RT}\right)}\right] (RT)^{\alpha+\beta+\gamma+\delta} C_A^{\alpha} C_B^{\beta} C_C^{\gamma} C_D^{\delta}}{F_{0_A}} \tag{3.6}$$

After that, in order to find the concentrations of each species, Equation 3.8 is written. The change in total volumetric flow rate due to the differences in stoichiometric coefficients between reactants and products was taken into account by adding ε to Equation 3.8, which represents the ratio of change in total number of moles for complete conversion to the total moles fed. In addition, if more than one reaction occurs in the reactor, the extent of reaction ξ should be taken into account.

$$\varepsilon = \frac{\sum_j^{\#\, of\ reactions} \sum_i^{\#\, of\ reactants} \varphi_{i,j} \xi_j}{\sum_j^{\#\, of\ reactions} \varphi_{A,j} \xi_j} x_{0_A} \tag{3.7}$$

$$C_i = C_{0_A} \frac{\frac{F_{0_i}}{F_{0_A}} - X_A \frac{\sum_j^{\#\, of\ reactions} \varphi_{i,j}\xi_j}{\sum_j^{\#\, of\ reactions} \varphi_{A,j}\xi_j}}{1 + \varepsilon X_A} \tag{3.8}$$

Where;

φ_i = Stoichiometric coefficient of species

x_i = mole fraction of species

4. RESULTS AND DISCUSSION

The aim of this study is to construct a FLUENT-based mathematical model of a Demo-scale fuel processor, which will be used as the base model to obtain the optimum operating parameters of a Demo-FP that produces sufficient amount of PEM-grade H_2, having CO concentration below 100 ppm, from methane in amount enough to feed a 1 kW PEMFC. Additionally, the established mathematical model will be also used as a starting point for the control model of the Demo-FP. The fuel processor system has three catalytic parts in series; OSR, WGS and PROX. Our group had been developed catalysts, tested their performance, and derived reliable kinetic expressions for the catalysts having the highest performance for all the FP reactions. Thus, at the starting point of the current study, both the performance test results *(ie. activity and selectivity data that had been obtained for ca. 75-250 mg. catalyst bed for various reaction conditions)* and kinetic expression derived based on kinetic studies *(ie. power law-type expression obtained based on kinetic tests performed at very low residence time, W/F, range by using catalyst amounts in 10-20 mg range)* for each reaction over the specific catalyst were available.

4.1. Modeling of Performance Tests and Validating Kinetic Expressions

In the first part of the current study, the power law type kinetic expressions obtained for the FP reactions were corrected through minimizing the difference between experimentally obtained performance test results that had been obtained previously and the results of the mathematical model formed in the current study for the same reaction conditions. In mathematical modeling of each reactor, experimentally determined power law-type kinetic expression, which had been obtained previously for the catalyst of each reaction, were used. Then, for each reactor, a comparative analysis was made between the experimental and calculated performance test results, and the kinetic expression for each reaction over its specific catalyst was corrected such as to minimize the difference between experimental and calculated values for the same performance test conditions. There our aim was to guarantee the reliability of the power law type kinetics via eliminating any possible effects may come from an order of magnitude difference in the amount of catalyst used between kinetic and performance tests. The ultimate output of the first part are the Fluent-

based models, which include corrected power-law kinetics, for the individual OSR, WGS and PROX reactors to be used in both FPP and Demo-FP models.

4.1.1. OSR Performance Tests

First stage of the reactor modelling is to find the catalyst bed length, and in order to calculate the bed length of 150 mg catalyst used in OSR performance tests, reactor diameter and density of the catalyst must be known. Inner and outer diameter of the reactor are tabulated in Table 3.1. Since all the reaction(s) takes place inside the reactor, the inner diameter of 0.46 cm -of the ¼ inch OD reactor- was taken as "the diameter of reactor". From Table 3.2, density of 0.2Pt-10Ni/δ-Al_2O_3, which is the catalyst designed, developed and optimized by our group for OSR reactor, is measured as 0.77 g cm^{-3}. Upon the insertion of the values, Equation 4.1 gave the bed length as 1.17 cm.

$$L = \frac{W}{\rho\, A} = \frac{0.15}{0.77 * \pi \left(\frac{0.46}{2}\right)^2} = 1.17\ cm \tag{4.1}$$

The power-law type kinetic expression of OSR reaction over 0.2Pt-10Ni/δ-Al_2O_3 that had been proposed by Erdinç (2014) were used in the current study; the form of the kinetic expression and the parameters calculated were presented in Eq. 4.2 and Table 4.1, respectively.

$$-r_{CH_4} = \left[k_0 (RT)^{\alpha+\beta+\gamma} e^{\left(\frac{-E_A}{RT}\right)}\right] C_{CH_4}^{\alpha} C_{O_2}^{\beta} C_{H_2O}^{\gamma} \tag{4.2}$$

The units of k_0 and E_A were corrected by adding density value (Table 3.2). Since there is no way to add $(RT)^{\alpha+\beta+\gamma}$ expression to Fluent, it was incorporated to k0 value by taking T as 623, 673, 723, 773 K and R as 8.314 L kPa K^{-1} mol^{-1}, and tabulated in Table 4.2. Consequently, the power-law type rate expression for 623 K becomes;

$$-r_{CH_4} = 1.09x10^{10} e^{\left(\frac{-31990}{8.314 * 623}\right)} C_{CH_4}^{0.81} C_{O_2}^{1.6} C_{H_2O}^{0.44} \tag{4.3}$$

Table 4.1. Estimated rate parameters for methane OSR over 0.2Pt-10Ni/δ-Al_2O_3 catalyst (Erdinç, 2014)

Parameter	Estimate	Unit
k_0	0.366	μmol mgcat^{-1} s^{-1} kPa$^{-2.85}$
E_A	31.99	kJ mol^{-1}
α	0.81	-
β	1.6	-
γ	0.44	-

Table 4.2. Modified rate expression parameters for methane OSR over 0.2Pt-10Ni/δ-Al_2O_3 catalyst

Parameter	Estimate	Unit
k_0 (for 623 K)	1.09 x 10^{10}	kmol m^{-3} s^{-1}
k_0 (for 673 K)	1.35 x 10^{10}	kmol m^{-3} s^{-1}
k_0 (for 723 K)	1.66 x 10^{10}	kmol m^{-3} s^{-1}
k_0 (for 773 K)	2.01 x 10^{10}	kmol m^{-3} s^{-1}
E_A	3.2 x 10^7	J kmol^{-1}

In OSR reactor, there are more than one reaction take place. It is assumed that, more than 10 reactions may occur simultaneously in OSR reactor (Shekhawat *et al.*, 2011); but most of them occur at a very low level, therefore they can be crossed out. Steam reforming producing CO and CO_2, partial and total oxidation and water-gas shift reactions are the main reactions of the oxidative steam reforming of methane over 0.2Pt-10Ni/δ-Al_2O_3 (Table 4.3). Since these 5 reactions take place simultaneously and the available rate expression had been derived for the lumped overall reaction, showing the activity in terms of rate of consumption of methane, the composition of the OSR product needed further calculations taking extent of reactions in account.

As the rate of every reaction vary with inlet composition, residence time and temperature through individual activation energy, the reaction selectivity varies. Thus, every experiment

must be evaluated separately and the selectivities calculated can only be used for the experiments with the same temperature, inlet composition and residence time.

Table 4.3. Main reactions take place in OSR reactor

Reaction Type	Reaction Formula
CO producing SR	$CH_4 + H_2O \leftrightarrow CO + 3\,H_2$
CO_2 producing SR	$CH_4 + 2\,H_2O \leftrightarrow CO_2 + 4\,H_2$
TOX	$CH_4 + 2\,O_2 \leftrightarrow CO_2 + 2\,H_2O$
POX	$CH_4 + 1/2\,O_2 \leftrightarrow CO + 2\,H_2$
WGS	$CO + H_2O \leftrightarrow CO_2 + H_2$

In order to find the selectivities of the reactions, the extent of reaction, ξ, must be taken into account. The extent of reactions can be calculated from the difference in molar flow rates between outlet and inlet (F_o and F_i).

$$F_{out_i} - F_{in_i} = \sum_{j}^{\#\,of\ reactions} \varphi_{i,j}\xi_j \tag{4.4}$$

In OSR reactor, 5 reactions take place involving 7 species; methane (CH_4), oxygen (O_2), water (H_2O), carbon monoxide (CO), carbon dioxide (CO_2), hydrogen (H_2) and helium (He). In order to calculate the selectivities of 5 reactions, knowing inlet and outlet molar flow rates of 5 species is sufficient. Since He is an inert gas and outlet molar flow rate of H_2O cannot be measured by neither GC nor MS; CH_4, O_2, CO, CO_2 and H_2 flows were used in calculation. From inlet and outlet molar flow rates of 5 species, a 5x1 matrix, from stoichiometric coefficients of species in 5 reactions, a 5x5 matrix and from extent of reaction of 5 reactions, a 5x1 matrix were formed (Equation 4.5).

The performance test results of Başar *et al.* were used for molar flow rates of inlet and outlet streams. Equation 4.5 was solved by taking the inverse of 5x5 matrix in MATLAB. As the coefficient matrix is square, ie. the matrix is close to singularity, pseudo-inverse function was used to solve the equation. It should be noted that the use of pseudo-inverse function results in 10% error margin in extent of reactions.

$$\begin{bmatrix} F_{o_{CH_4}} - F_{i_{CH_4}} \\ F_{o_{O_2}} - F_{i_{O_2}} \\ F_{o_{CO}} - F_{i_{CO}} \\ F_{o_{CO_2}} - F_{i_{CO_2}} \\ F_{o_{H_2}} - F_{i_{H_2}} \end{bmatrix} = \begin{bmatrix} -1 & -1 & -1 & -1 & 0 \\ 0 & 0 & -2 & -0.5 & 0 \\ 1 & 0 & 0 & 1 & -1 \\ 0 & 1 & 1 & 0 & 1 \\ 3 & 4 & 0 & 2 & 1 \end{bmatrix} * \begin{bmatrix} \xi_1 \\ \xi_2 \\ \xi_3 \\ \xi_4 \\ \xi_5 \end{bmatrix} \tag{4.5}$$

Molar flow rate of H_2O at the outlet was unknown for this case, but the total mass flow rates of both inlet and outlet streams are known. Therefore, in order to calculate the stoichiometric coefficient of H_2O, the mass flow rate of H_2O was calculated by subtracting the mass flow rate of inlet from the mass flow rate of outlet and dividing it by molecular weight of H_2O. Finally, stoichiometric coefficients of every species in total reaction (except He) were calculated by Equation 4.6, normalized for CH_4 and tabulated in Table 4.6.

$$\begin{bmatrix} \varphi_{CH_4} \\ \varphi_{O_2} \\ \varphi_{H_2O} \\ \varphi_{CO} \\ \varphi_{CO_2} \\ \varphi_{H_2} \end{bmatrix} = \begin{bmatrix} -1 & -1 & -1 & -1 & 0 \\ 0 & 0 & -2 & -0.5 & 0 \\ -1 & -2 & 2 & 0 & -1 \\ 1 & 0 & 0 & 1 & -1 \\ 0 & 1 & 1 & 0 & 1 \\ 3 & 4 & 0 & 2 & 1 \end{bmatrix} * \begin{bmatrix} \xi_1 \\ \xi_2 \\ \xi_3 \\ \xi_4 \\ \xi_5 \end{bmatrix} \tag{4.6}$$

After obtaining extent of reaction of every test, the inlet conditions were entered Fluent. The performance tests of Başar *et al.* were used for this purpose (Table 4.5).

Table 4.4. List of performance test parameters over 0.2Pt-10Ni/δ-Al_2O_3 catalyst

Parameter	**Value**	**Unit**
Inlet Temperature	25	ºC
Inlet Pressure	1	bar
Catalyst Amount	150	mg
Catalyst Bed Length	1.17	cm

Table 4.5. List of performance tests over 0.2Pt-10Ni/δ-Al_2O_3 catalyst (Başar *et al.*)

Exp. #	$T_{Reactor}$ (°C)	S/C	W/F (mgcat min/ml)	Inlet Compositions (ml/min)				
				CH_4	O_2	H_2O	He	Total
1	350	2.25	1.68	13.70	9.30	31.10	35.00	89.10
2	350	3.00	1.50	13.70	9.30	42.00	35.00	100.00
3	350	5.00	1.19	13.70	9.30	68.50	35.00	126.50
4	350	6.00	1.07	13.70	9.30	82.60	35.00	140.60
5	400	2.25	1.68	13.70	9.30	31.10	35.00	89.10
6	400	3.00	1.50	13.70	9.30	42.00	35.00	100.00
7	400	5.00	1.19	13.70	9.30	68.50	35.00	126.50
8	400	6.00	1.07	13.70	9.30	82.60	35.00	140.60
9	450	2.25	1.68	13.70	9.30	31.10	35.00	89.10
10	450	3.00	1.50	13.70	9.30	42.00	35.00	100.00
11	450	5.00	1.19	13.70	9.30	68.50	35.00	126.50
12	450	6.00	1.07	13.70	9.30	82.60	35.00	140.60
13	500	2.25	1.68	13.70	9.30	31.10	35.00	89.10
14	500	3.00	1.50	13.70	9.30	42.00	35.00	100.00
15	500	5.00	1.19	13.70	9.30	68.50	35.00	126.50
16	500	6.00	1.07	13.70	9.30	82.60	35.00	140.60

The simulation of performance tests was carried out by both Fluent and Polymath, and both calculated and experimental results were tabulated in Table 4.7. It can be clearly seen from the Table that there is a very nice match between values calculated by Fluent and Polymath. As porosity, viscous resistance and inertial resistance were not been incorporated in Fluent model at this stage, the exact match between Polymath and Fluent results confirm the correctness of the basic Fluent model lacks those effects. Though the experimental results are close to calculated ones but the differences are not ignorable.

Table 4.6. List of stoichiometric coefficients of performance tests

Exp. #	Stoichiometric Coefficient					
	CH_4	O_2	H_2O	CO	CO_2	H_2
1	1.000	1.334	0.686	0.018	0.982	1.314
2	1.000	1.310	0.642	0.022	0.978	1.358
3	1.000	1.217	0.465	0.031	0.969	1.535
4	1.000	1.208	0.446	0.030	0.970	1.554
5	1.000	1.205	0.440	0.030	0.970	1.560
6	1.000	1.157	0.341	0.027	0.973	1.659
7	1.000	1.075	0.172	0.021	0.978	1.828
8	1.000	1.028	0.082	0.027	0.973	1.918
9	1.000	1.029	0.118	0.060	0.940	1.882
10	1.000	0.977	0.009	0.055	0.945	1.991
11	1.000	0.859	0.227	0.055	0.944	2.227
12	1.000	0.785	0.367	0.063	0.937	2.367
13	1.000	0.767	0.288	0.178	0.822	2.288
14	1.000	0.732	0.384	0.151	0.849	2.384
15	1.000	0.622	0.620	0.136	0.863	2.620
16	1.000	0.572	0.738	0.119	0.881	2.738

The reasons for the mismatch between experimental and calculated conversion values might be stated as follows; firstly, in the experiments it was assumed that the temperature of the catalyst bed is exactly equal to outer surface temperature of the reactor. In reality, there may be small differences for the performance tests due to the heat transfer between catalyst particles, and the inner temperature may be slightly lower or higher than the temperature measured from the outside depending on the experimental conditions used. On the other hand, the kinetic expression had been derived on the basis of the experimental results obtained over 10 and 15 mg catalysts, and for that very tiny catalyst amounts, as the bed length is negligible (or very limited), there should not be a heat transfer between particles that could yield inner-outer temperature difference for the reactor.

Table 4.7. Fluent and Polymath CH_4 conversion results of performance tests over 0.2Pt-10Ni/δ-Al_2O_3 catalyst

Exp. #	T(C)	Polymath CH_4 Conversion (%)	Fluent CH_4 Conversion (%)	Experimental CH_4 Conversion (%)
1	350	50.59	50.65	43.43
2	350	51.24	51.34	46.73
3	350	54.11	54.30	46.73
4	350	53.85	53.65	45.30
5	400	56.07	56.23	49.68
6	400	58.17	58.18	52.02
7	400	61.69	61.65	56.74
8	400	64.50	64.12	55.82
9	450	65.49	65.34	58.38
10	450	68.63	68.61	62.61
11	450	76.24	76.34	68.03
12	450	81.07	81.09	69.21
13	500	86.44	86.31	80.83
14	500	89.43	89.12	85.46
15	500	96.94	96.34	91.97
16	500	98.56	98.94	94.23

(ii) it was already mentioned above that, the use of pseudo-inverse function resulted in ±10% error margin in the extent of reactions. If the stoichiometric coefficients calculated by MATLAB was compared with the ones calculated by subtracting the outlet molar flow rate of a species from inlet are analyzed, it is evident that, there are errors involved in MATLAB calculated-stoichiometric coefficients. However, a closer look to the system shows that, the error in hydrogen stoichiometric coefficients are much less than that of methane stoichiometric coefficients. Therefore, for OSR system, the hydrogen production will be used as the calculation base instead of methane conversion. The experimental, and Fluent and Polymath results on hydrogen production for performance tests were tabulated in Table 4.8.

Table 4.8. Fluent and Polymath H_2 production results of performance tests over 0.2Pt-10Ni/δ-Al_2O_3 catalyst

Exp. #	T (C)	Polymath Flow Rate of H_2 (moles/s)	Fluent Flow Rate of H_2 (moles/s)	Experimental Flow Rate of H_2 (moles/s)
1	350	6.13×10^{-6}	6.13×10^{-6}	6.12×10^{-6}
2	350	6.41×10^{-6}	6.41×10^{-6}	6.83×10^{-6}
3	350	7.63×10^{-6}	7.63×10^{-6}	7.94×10^{-6}
4	350	7.64×10^{-6}	7.64×10^{-6}	8.10×10^{-6}
5	400	8.04×10^{-6}	8.04×10^{-6}	8.00×10^{-6}
6	400	8.90×10^{-6}	8.90×10^{-6}	8.93×10^{-6}
7	400	1.02×10^{-5}	1.02×10^{-5}	1.07×10^{-5}
8	400	1.09×10^{-5}	1.09×10^{-5}	1.18×10^{-5}
9	450	1.14×10^{-5}	1.14×10^{-5}	1.13×10^{-5}
10	450	1.26×10^{-5}	1.26×10^{-5}	1.27×10^{-5}
11	450	1.55×10^{-5}	1.55×10^{-5}	1.60×10^{-5}
12	450	1.74×10^{-5}	1.74×10^{-5}	1.81×10^{-5}
13	500	1.82×10^{-5}	1.82×10^{-5}	1.81×10^{-5}
14	500	1.95×10^{-5}	1.95×10^{-5}	1.98×10^{-5}
15	500	2.31×10^{-5}	2.31×10^{-5}	2.49×10^{-5}
16	500	2.46×10^{-5}	2.46×10^{-5}	2.72×10^{-5}

(iii) The main reason for using Fluent in this study is to observe the effect of porous media. In calculating kinetic expression, no effect of porous media was taken into account, in other words, the system assumed to have no resistance against flowing fluid. It is assumed this is the case when the porosity reaches 100%. In reality, the porosity less than 100% and a decrease in porosity means reduced empty spaces between the catalyst particles. It results in reduction in active surface area and ultimately reduces the reaction rate. Fluent can take the effect of porous body into account, while Polymath cannot. Therefore, if the parameters concerning porous body are taken into account in Fluent model, it is expected that Fluent and Polymath results should not match while Fluent model results should come closer to experimental ones.

The porosity, viscous resistance and inertial resistance were calculated through the use of Equations 4.7-4.9, respectively. From Table 3.2, bulk density of catalyst is found as 0.77 g/cm^3, and solid density for 0.2Pt-10Ni/δ-Al_2O_3 catalyst was taken from the literature as 4.35 g/cm^3. Viscous resistance and inertial resistance values were calculated by using the formulas present in ANSYS Fluent Theory Guide (Equation 4.8 and 4.9).

$$\varepsilon = 1 - \frac{\rho_b}{\rho_s} = 1 - \frac{0.77 \text{ g cm}^{-3}}{4.35 \text{ g cm}^{-3}} = 0.823 \tag{4.7}$$

$$\frac{1}{k} = \frac{1}{\left(\frac{D_p^2 \varepsilon^3}{150\,(1-\varepsilon)^2}\right)} = \frac{1}{\left(\frac{(0.0003\,m)^2\,(0.823)^3}{150\,(1-0.823)^2}\right)} = 9.37x10^7 m^{-2} \tag{4.8}$$

$$c = \frac{3.5\,(1-\varepsilon)}{D_p\,\varepsilon^3} = \frac{3.5\,(1-0.823)}{0.0003 \text{ m}\ (0.823)^3} = 3704.82\,m^{-1} \tag{4.9}$$

In order to fix the errors caused by abovementioned reasons, a correction factor is added to the reaction rate along with the porous body parameters (Table 4.9). A series of trial and error calculations were carried out to find a correction factor valid in the range of 350-500 ºC; the correction factor that minimized the error was obtained as 1.5. The correction factor was directly multiplied with k_0 value and entered the Fluent system. The results were tabulated in Table 4.10.

Table 4.9. Porous body parameters of 0.2Pt-10Ni/δ-Al_2O_3 catalyst

Parameter	**Value**	**Unit**
Porosity	0.823	-
Viscous Resistance	9.37 x 10^{-7}	1/m^2
Inertial Resistance	3704.8186	1/m

Experimental CH_4 conversion and H_2 production increase with the increase in temperature and S/C feed ratio. The values presented in Table 4.10 show that Fluent based calculational results are in accordance with the experimental results. However, it should be noted that the Fluent based conversion results are always bigger than those obtained in the

experiments. As the stoichiometric 5x5 matrix is singular, it is unclear whether the reason for this gap is caused by the temperature difference between the catalyst surface and the reactor, or by singularity of matrix. Since the values revealed that the gaps between experimental and calculated H_2 flow rates are very small, even negligible in some cases, one can consider H_2 flow as a reliable basis.

Table 4.10. Fluent H_2 production and CH_4 conversion with 1.5 correction factor and porous body parameters results of performance tests over 0.2Pt-10Ni/δ-Al_2O_3 catalyst

Exp. #	**T (C)**	**Fluent CH_4 Conversion (Corrected) (%)**	**Experimental CH_4 Conversion (%)**	**Fluent Flow Rate of H_2 (Corrected) (moles/s)**	**Experimental Flow Rate of H_2 (moles/s)**
1	350	50.77	43.43	6.22×10^{-6}	6.12×10^{-6}
2	350	51.43	46.73	6.51×10^{-6}	6.83×10^{-6}
3	350	54.16	46.73	7.76×10^{-6}	7.94×10^{-6}
4	350	53.80	45.30	7.76×10^{-6}	8.10×10^{-6}
5	400	56.28	49.68	8.17×10^{-6}	8.00×10^{-6}
6	400	58.20	52.02	8.97×10^{-6}	8.93×10^{-6}
7	400	61.62	56.74	1.05×10^{-5}	1.07×10^{-5}
8	400	63.51	55.82	1.13×10^{-5}	1.18×10^{-5}
9	450	65.64	58.38	1.15×10^{-5}	1.13×10^{-5}
10	450	68.67	62.61	1.27×10^{-5}	1.27×10^{-5}
11	450	76.30	68.03	1.59×10^{-5}	1.60×10^{-5}
12	450	81.22	69.21	1.79×10^{-5}	1.81×10^{-5}
13	500	86.21	80.83	1.84×10^{-5}	1.81×10^{-5}
14	500	89.10	85.46	1.98×10^{-5}	1.98×10^{-5}
15	500	96.72	91.97	2.37×10^{-5}	2.49×10^{-5}
16	500	99.06	94.23	2.52×10^{-5}	2.72×10^{-5}

The results presented in Table 4.10 revealed that, the difference between experimental and Fluent based results are very low in case of proper porous body parameters and a correction factor are introduced to the model. It should be additionally noted that at

reaction temperatures 400 and 450 ^{o}C, the difference becomes practically zero, whereas at 500 ^{o}C, the results tend to deviate. The most probable reason behind this is the fact that methane OSR rate expression was obtained from the tests performed at 375 ^{o}C; as the OSR is highly temperature sensitive reaction having E_A value constant only for 50-75°C temperature intervals, when the reaction temperature deviates from 375 ^{o}C, there may be error involved in the model results as the rate expression parameters are kept fixed.

Table 4.11. Fluent outlet composition of CO results of performance tests over 0.2Pt-10Ni/δ-Al_2O_3 catalyst

Exp. #	**T (C)**	**Fluent CO Mole Fraction (%)**	**Experimental CO Mole Fraction (%)**
1	350	0.138	0.132
2	350	0.157	0.149
3	350	0.177	0.175
4	350	0.162	0.156
5	400	0.243	0.245
6	400	0.192	0.206
7	400	0.136	0.138
8	400	0.163	0.159
9	450	0.549	0.555
10	450	0.464	0.478
11	450	0.422	0.429
12	450	0.449	0.471
13	500	1.920	2.057
14	500	1.574	1.643
15	500	1.229	1.284
16	500	1.063	1.034

One of the main targets of a Demo-scale fuel processor system is CO level at the outlet must not exceed 100 ppm. Therefore, it is essential to compare and analyze the CO levels obtained from experiments and through the use of Fluent model. CO mole fraction

values in the OSR product (Table 4.11) show that, similar to the case for H_2 production rates, the experimental and model based results are very close.

It is evident from the comparative analysis of experimental and model based H_2 flow and CO concentration date that through the use of proper correction factor and bed porosity, Fluent-based OSR model is reliable to be used as the part of FPP and Demo-FP models given that 0.2Pt-10Ni/δ-Al_2O_3 is considered as the catalyst for methane OSR.

4.1.2. WGS Performance Tests

The catalyst bed length of the WGS reactor was calculated first. Specifications of the reactor were taken from Table 3.1 and density of 1Pt-0.5Re-1V/CeO_2 WGS catalyst was used as 0.93 g/cm^3 (Table 3.2). Equation 4.10 yields the catalyst bed length as 0.485 cm.

$$L = \frac{W}{\rho\, A} = \frac{0.075}{0.93 * \pi \left(\frac{0.46}{2}\right)^2} = 0.485\ cm \tag{4.10}$$

The power-law type kinetic expression for WGS over 1Pt-0.5Re-1V/CeO_2, which was obtained by Yumru (2017), was used in the calculations. Due to the equilibrium nature of the reaction, a parameter β', which is a function of partial pressure of species at inlet, was added to the WGS rate expression.

$$-r_{CO} = \left[k_0 (RT)^{\alpha+\beta+\gamma+\delta+\varepsilon} e^{\left(\frac{-E_A}{RT}\right)}\right] C_{CO}^{\alpha} C_{H_2O}^{\beta} C_{H_2}^{\gamma} C_{CO_2}^{\gamma} C_{CH_4}^{\varepsilon} (1-\beta') \tag{4.11}$$

$$\beta' = \frac{1}{K_{eq}} \frac{P_{H_2} P_{CO_2}}{P_{CO} P_{H_2O}} \tag{4.12}$$

$$K_{eq} = \exp\left(\frac{4577.8}{T} - 4.33\right) \tag{4.13}$$

As in the case of OSR reaction, the power law type kinetic expressions obtained for WGS were corrected through minimizing the difference between experimentally obtained

performance test results that had been obtained previously and the results of the mathematical model formed in the current study for the same reaction conditions. As it is assumed that there is no side reaction in WGS reactor, there is no need for selectivity calculation. The reaction conditions used in the performance tests were taken from Kesim (2017). The inlet conditions for all sets along with (1-β') factors were tabulated.

Table 4.12. Estimated rate expression parameters over 1Pt-0.5Re-1V/CeO_2 catalyst (Yumru, 2017)

Parameter	Estimate	Unit
k_0	29209	μmol $gcat^{-1}$ s^{-1} $kPa^{-0.49}$
E_A	28.215	kJ mol^{-1}
α	0.82	-
β	0.31	-
γ	-0.29	-
δ	-0.35	-
ε	0.002	-

Table 4.13. Modified rate expression parameters over 1Pt-0.5Re-1V/CeO_2 catalyst

Parameter	Estimate	Unit
k_0	1794.76	kmol m^{-3} s^{-1}
E_A	2.82 x 10^7	J $kmol^{-1}$

Table 4.16 shows the results of the experimental performance tests along with the ones calculated by Fluent, and Polymath in terms of CO conversion. It should be noted that the effect of porosity was ignored at that stage. As expected, the conversion values obtained from Fluent and Polymath simulations are very close. On the other hand, experimental results obtained by Kesim (2017) are much different than the results calculated by Fluent. The most probable reasons for the differences are; exclusion of bed porosity in calculations and suppression of conversion during performance tests due to equilibrium nature of the reaction, which exceeds the correction of β' factor at higher conversions.

Table 4.14. List of performance tests over 1Pt-0.5Re-1V/CeO_2 catalyst (Kesim, 2017)

Exp. #	$T_{Reactor}$ (°C)	(1-β')	H_2O/CO	Inlet Molar Compositions (%)				
				CO	H_2O	H_2	CO_2	Ar
1	300	0.8952	16.2	2.1	34.1	23.7	12.3	27.8
2	300	0.9499	6.7	4.9	32.7	30	10.4	22
3	350	0.8009	16.2	2.1	34.1	23.7	12.3	27.8
4	350	0.9048	6.7	4.9	32.7	30	10.4	22
5	400	0.6564	16.2	2.1	34.1	23.7	12.3	27.8
6	400	0.8356	6.7	4.9	32.7	30	10.4	22

Table 4.15. List of performance tests over 1Pt-0.5Re-1V/CeO_2 catalyst

Parameter	Value	Unit
Inlet Temperature	25	°C
Inlet Pressure	1	bar
Catalyst Amount	75	mg
Catalyst Bed Length	0.485	cm
Flow Rate	150	ml min^{-1}

Table 4.16. Fluent and Polymath CO conversion results of performance tests over 1Pt-0.5Re-1V/CeO_2 catalyst

Exp. #	$T_{Reactor}$ (°C)	Polymath CO Conversion (%)	Fluent CO Conversion (%)	Experimental CO Conversion (%)
1	300	93.36	85.30	40.63
2	300	88.24	86.42	29.93
3	350	99.11	93.18	59.34
4	350	97.76	95.09	67.73
5	400	99.93	88.57	51.26
6	400	99.87	91.54	61.6

Through minimization of differences between experimental and calculated conversion values, the correction factor to be used in Fluent model was obtained as 0.33. The conversion results calculated by Fluent upon the inclusion of correction factor and porous body parameters (Table 4.17) are presented in Table 4.18. As it can be seen from the Table 4.18, the difference between experimental and corrected Fluent results were much less than the errors between experimental and non-corrected Fluent results.

Table 4.17. Porous body parameters of 1Pt-0.5Re-1V/CeO_2 catalyst

Parameter	**Value**	**Unit**
Porosity	0.878	-
Viscous Resistance	3.63×10^{-7}	$1/m^2$
Inertial Resistance	2092.4	1/m

Table 4.18. Fluent CO conversion with 0.33 correction factor and porous body parameters results of performance tests over 1Pt-0.5Re-1V/CeO_2 catalyst

Exp. #	**$T_{Reactor}$ (ºC)**	**Fluent CO Conversion (Corrected) (%)**	**Experimental CO Conversion (%)**
1	300	45.24	40.63
2	300	37.08	29.93
3	350	59.90	59.34
4	350	57.37	67.73
5	400	57.82	51.26
6	400	66.17	61.6

In conclusion, even though the calculation results of methane OSR seems more accurate than those of WGS; it can be safely assumed that, upon the correction reducing the error margin to $^{\pm}$10%, the Fluent model results in a highly reliable performance estimation for the WGS reactor and, consequently, the Fluent-based WGS model is reliable to be used

as the part of FPP and Demo-FP models given that 1Pt-0.5Re-1V/CeO_2 is considered as the catalyst for WGS reactor.

4.1.3. PROX Performance Tests

The catalyst bed length of the PROX reactor was calculated first. Specifications of the reactor were taken from Table 3.2, and density of 1Pt-0.25Sn/AC PROX catalyst was used as 0.44 g/cm^3 (Table 3.2). Through the use of Equation 4.10 the catalyst bed length for the amount of catalyst used in performance tests, 250 mg, was calculated as 3.42 cm.

$$L = \frac{W}{\rho\, A} = \frac{0.25}{0.44 * \pi \left(\frac{0.46}{2}\right)^2} = 3.4268\ cm \tag{4.14}$$

In the mathematical, Polymath and Fluent based, models, the power law type rate expression obtained by Eropak and Aksoylu (2017) was used. According to their findings; under the flow of realistic gas mixture mimicking WGS outlet of a fuel processor, the PROX reaction kinetics can be well represented by a simple power law type model having only CO and O_2 terms. (Equation 4.15) (Table 4.19). It should be noted that k_0 and E_A values were modified to have Fluent compliant units (Table 4.20).

$$-r_{CO} = \left[k_0 (RT)^{\alpha+\beta} e^{\left(\frac{-E_A}{RT}\right)}\right] C_{CO}^{\alpha} C_{O_2}^{\beta} \tag{4.15}$$

Table 4.19. Estimated rate expression parameters over 1Pt-0.25Sn/AC catalyst (Eropak and Aksoylu, 2017)

Parameter	Estimate	Unit
k_0	5.83 x 10^7	µmol mgcat^{-1} min^{-1} kPa$^{0.1}$
E_A	54.3	kJ mol^{-1}
α	0.47	-
β	-0.57	-

Table 4.20. Modified rate expression parameters over 1Pt-0.25Sn/AC catalyst

Parameter	Estimate	Unit
k_0	19049.29	kmol m^{-3} s^{-1}
E_A	5.43 x 10^7	J $kmol^{-1}$

In verification of the kinetic model, the performance test results had been presented by Çağlayan *et al.* (2011) were used. In their study, 4 different temperature levels, 110, 115, 125 and 135 ºC, were used during the tests. As the kinetic model formed based on the tests performed at 110 ºC by Eropak and Aksoylu (2017), which had been confirmed as the optimum temperature yielding the highest CO conversion selectively in the performance tests; the model in the current study was only used to simulate the performance tests conducted at 110 ºC. The reaction conditions used in the performance tests are tabulated in Table 4.21. It should be noted that; each test was performed over 250 mg freshly reduced catalyst under a fixed gas inlet flow rate as 100 ml/min where He was used as the balance inert gas (Table 4.22).

Table 4.21. List of performance tests over 1Pt-0.25Sn/AC catalyst (Çağlayan *et al.*, 2011)

Exp. #	**$T_{Reactor}$ (ºC)**	**O/CO**	**Inlet Flow Rates (ml/min)**						
			CO	**O_2**	**H_2**	**CO_2**	**CH_4**	**H_2O**	**He**
1	110	2	1	1	60	0	0	0	38
2	110	2.5	1	1.25	60	0	0	0	37.75
3	110	2	1	1	60	15	0	10	13
4	110	2.5	1	1.25	60	15	0	10	12.75
5	110	2	1	1	60	0	3	0	35
6	110	2.5	1	1.25	60	0	3	0	34.75

In PROX performance tests, apart from O/CO ratio, effects of CO_2, CH_4, H_2O to the conversion were also investigated. Performance test results showed that, change in molar flow rate of CO_2, CH_4, H_2O virtually had no effect in conversion (Table 4.23). The Fluent and Polymath models based simulation results also confirmed those findings. Rather small differences between the results of performance tests and porous body effect free Fluent

model for the same inlet conditions hinted that the effect of porosity is small compared to that in OSR and WGS models.

Table 4.22. List of performance tests over 1Pt-0.25Sn/AC catalyst

Parameter	Value	Unit
Inlet Temperature	25	^{o}C
Inlet Pressure	1	bar
Catalyst Amount	250	mg
Catalyst Bed Length	0.2056	cm
Flow Rate	100	ml min^{-1}

Table 4.23. Fluent and Polymath CO conversion results of performance tests over 1Pt-0.25Sn/AC catalyst

Exp. #	$T_{Reactor}$ (^{o}C)	Polymath CO Conversion (%)	Fluent CO Conversion (%)	Experimental CO Conversion (%)
1	110	99.92	99.99	87.20
2	110	79.89	90.79	91.17
3	110	99.92	99.99	86.23
4	110	79.89	89.32	70.48
5	110	99.92	99.99	87.37
6	110	79.89	89.12	82.09

Table 4.24. Porous body parameters of 1Pt-0.25Sn/AC catalyst

Parameter	Value	Unit
Porosity	0.78	-
Viscous Resistance	2.44×10^{8}	$1/m^{2}$
Inertial Resistance	6468.57	1/m

Table 4.25. Fluent CO conversion with porous body parameters results of performance tests over 1Pt-0.25Sn/AC catalyst

Exp. #	$T_{Reactor}$ (°C)	Fluent CO Conversion (Corrected) (%)	Experimental CO Conversion (%)
1	110	90.49	87.20
2	110	79.75	91.17
3	110	90.87	86.23
4	110	81.22	70.48
5	110	90.28	87.37
6	110	81.60	82.09

By following the same methodology that were used in OSR and WGS cases, a trial and error procedure was performed to find an optimum correction factor minimizing the difference between the results of performance tests and Fluent-based model having porosity effect; the analysis gave the correction factor as 1, which means there is essentially no need for a correction factor. Thus, the results validate the use of Fluent model with correction factor as '1' and 78% porosity for PROX reactor utilizing 1Pt-0.25Sn/AC catalyst in both FPP and Demo-FP models.

4.2. Modeling of Fuel Processor System

In the second part of the current study, first the fuel processor prototype (FPP) was modeled and its performance was simulated through the use of corrected kinetic models. In FPP model, FP reactors (OSR-WGS-PROX) having ¼ inch-OD were modeled in series along with their transfer lines. In this part of the study, 16 FPP simulations were performed by using the feed composition, temperature and W/F of the OSR reactor as had been used in the first part; those sets were previously used by Basar (2016) in OSR performance tests. On the other hand, as OSR and WGS outlets were used as the feeds of WGS and PROX reactors, respectively, for the serially following WGS and PROX reactors only the temperature and amount of catalyst was chosen in line with the conditions yielding best performance specs in individual performance tests. Then, in the second stage of this part, the same 16

simulations were performed for 1-inch OD of the reactors, which is the OD of the reactors has been planned to be used in Demo-FP, while the catalyst bed height of each reactor were kept fixed as in the case of ¼ inch reactors *(ie. the same bed height was used as in ¼ inch reactors)* and the catalyst amount was increased accordingly. There the flow rate of the OSR feed was increased such as to keep W/F of the OSR reactor the same as the ¼ inch case. At the final stage of this section, the reaction conditions and temperature combination yielding the best performance in terms of hydrogen production and CO level at the exit of the PROX reactor were selected; for those four selected sets, the catalyst amounts in the reactors increased while keeping the W/F fixed such as to satisfy the H_2 flow and CO impurity limit specifications of the Demo-FP outlet for feeding 1 kW PEMFC. The hydrogen flow rate and CO concentration limit were taken as 0.00272 moles/s (Berry, 2004) and 100 ppm, respectively. Though H_2 flowrate value varies from one source to another, all reported values are close. It should be noted that for the last two stages of FP simulations, powder form of the catalysts was used though especially for higher bed lengths this may lead to pressure drop during real operation, ie. Demo-FP performance tests. In both FPP and Demo-FP simulations, whenever all the oxygen present in OSR feed used up in OSR reactor for all sets, the oxygen needed in PROX reactor was added to the system at the entrance of PROX reactor.

4.2.1. Fuel Processor System with 0.25 Inch Reactor Diameter

In this part, the individual reactor models obtained in Section 4.1, which have corrected kinetic expressions, were used for OSR, WGS and PROX reactors. In FPP simulations, the reaction conditions for OSR reactor listed in Table 4.5, which were previously used by Basar (2016) in OSR performance tests over 0.2Pt-10Ni/δ-Al_2O_3 and in Section 4.1 of the current study in individual OSR simulations, were used.

As OSR and WGS outlets were used as the feeds of WGS and PROX reactors, respectively; for the serially following WGS and PROX reactors, only the temperature and amount of catalyst were chosen in line with the conditions yielding best performance specs in individual performance tests. For each WGS and PROX reactors, the temperature level that had yielded the highest catalyst performance in experimental studies was used.

In the study conducted by Kesim (2017), WGS performance data over 1Pt-0.5Re-1V/CeO_2 for 300-400 ^oC temperature interval were presented. The results of the performance tests showed that, the highest CO conversion levels had been reached at 350 ^oC. Accordingly, the kinetic tests had also been conducted by Yumru over the same catalyst at 350 ^oC. Based on the previous results, WGS reactor temperature were kept fixed at 350 ^oC for all 16 simulations in the current study.

As WGS reactor has OSR product as its feed, the feed flowrate (and consequently W/F) and H_2O/CO feed ratio of WGS reactor were imposed by OSR product flow and composition. Thus, in the simulations, only WGS reactor temperature and catalyst weight were specified. In all simulations, the amount of WGS catalyst was 75 mg, and reactor temperature was 350 ^oC. On the other hand, as WGS kinetics has β'factor, which is used to include equilibrium driven suppression of rate, that changes in response to a change in WGS inlet compositions; for each simulation, a (1-β') value was calculated for the corresponding OSR outlet composition. It should be noted that OSR product flow and compositions for the whole 16 simulation sets were known from the Fluent based model developed for OSR reactor and used in performance tests (see Section 4.1; OSR performance). The outlet stream compositions and their respective 1-β' values for the whole 16 simulations are tabulated in Table 4.26. As it can be seen from the table, 1-β' values are highly sensitive to residence time, ie. W/F ratio, of OSR reactor.

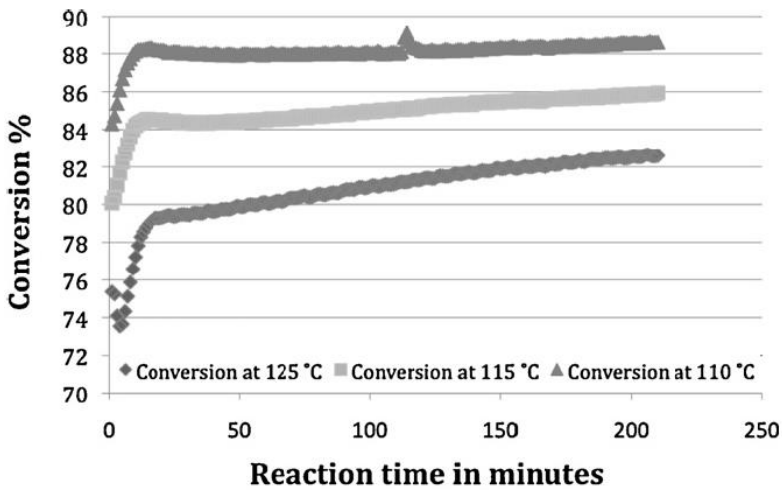

Figure 4.1. PROX performance of Pt–Sn/AC-N as CO conversion at O_2:CO = 1:1 (Çağlayan *et al.*, 2011)

In the article written by Çağlayan *et al.* on PROX performance of 1%Pt–0.25%Sn/AC-N, the reaction time based conversion trends at different temperature levels were presented (Figure 4.1). The trends clearly show that the highest PROX conversion levels had been reached at 110 ^{o}C. In accordance with the performance trends, the kinetic tests by Eropak and Aksoylu were conducted at 110 ^{o}C. As PROX reactor has WGS product as its feed, the feed flowrate (and consequently W/F) and H_2O/CO feed ratio of PROX reactor were imposed by WGS product flow and composition. Thus, in the simulations, only PROX reactor temperature and catalyst weight were specified. In all simulations, the amount of PROX catalyst was 250 mg, and reactor temperature was 110 ^{o}C.

Table 4.26. Outlet compositions of OSR performance tests over 0.2Pt-10Ni/δ-Al_2O_3 catalyst and (1-β') factors for WGS reaction over 1Pt-0.5Re-1V/CeO_2 catalyst

Exp. #	**T_{OSR} (^{o}C)**	**$(W/F)_{OSR}$ (mgcat min/ml)**	**OSR Outlet Composition (%)**							**(1-β') for WGS**
			CH_4	**O_2**	**H_2O**	**CO**	**CO_2**	**H_2**	**He**	
1	350	1.68	7.26	0.09	38.26	0.13	7.26	9.39	37.60	0.339
2	350	1.50	6.35	0.03	44.35	0.15	6.63	9.16	33.33	0.551
3	350	1.19	4.59	0.03	54.41	0.18	5.54	8.79	26.46	0.750
4	350	1.07	4.17	0.04	58.68	0.16	5.02	8.04	23.89	0.784
5	400	1.68	6.29	0.02	36.24	0.25	7.86	12.59	36.76	0.455
6	400	1.50	5.27	0.02	41.96	0.21	7.32	12.45	32.78	0.485
7	400	1.19	3.80	0.04	52.15	0.14	6.18	11.56	26.12	0.516
8	400	1.07	3.16	0.05	55.85	0.16	5.86	11.49	23.44	0.630
9	450	1.68	4.78	0.01	32.86	0.55	8.62	17.35	35.81	0.599
10	450	1.50	3.84	0.03	38.39	0.48	8.16	17.19	31.92	0.626
11	450	1.19	2.13	0.05	47.64	0.43	7.31	17.20	25.24	0.700
12	450	1.07	1.34	0.08	50.70	0.47	7.05	17.73	22.63	0.744
13	500	1.68	1.62	0.07	26.59	2.06	9.52	26.49	33.66	0.775
14	500	1.50	1.00	0.10	32.10	1.64	9.18	25.78	30.20	0.780
15	500	1.19	0.02	0.55	41.30	1.28	8.12	24.65	24.08	0.815
16	500	1.07	0.00	0.84	45.10	1.03	7.62	23.69	21.73	0.811

Table 4.27. Specifications of the FPP system utilizing 0.25-inch OD reactors

Parameter	Value	Unit
Inner diameter of a reactor	0.46	cm
Total length of a reactor	37	cm
Total length of mixing area	10	cm
Length of O_2 inlet	10	cm
Length of interface areas	1	cm
Length of OSR catalyst bed	1.17	cm
Catalyst amount of OSR reactor	150	mg
Temperature of OSR reactor	350-500	^oC
Length of WGS catalyst bed	0.485	cm
Catalyst amount of WGS reactor	75	mg
Temperature of WGS reactor	350	^oC
Length of PROX catalyst bed	3.43	cm
Catalyst amount of PROX reactor	250	mg
Temperature of PROX reactor	110	^oC
Inlet Temperature	25	^oC
Outlet Temperature	25	^oC
Inlet Pressure	1	bar

Upon choosing the operation parameters for all three reactors and performing the necessary calculations for reactor model parameters as well, the FPP system model to be used in simulations was established. Table 4.27 shows the specifications of the FPP system mode and Table 4.28 shows the inlet conditions of the runs. Three reactors were set up consecutively. Additionally, 1 cm long interface areas were added in between the reactors and an additional O_2 inlet stream was implemented before the PROX reactor with a mixing area enough to thwart the possible backflow.

The results of the 16 simulations performed by using the Fluent based FPP model are presented in Table 4.29. OSR conversions and H_2 production rates are the same as the performance test results of methane OSR presented in Section 4.1. Since the results clearly showed that the H_2 flow rates are, as expected, lower than necessary for 1kW PEMFC; a fuel

processor system involving reactors with larger diameter and packed with higher amount of catalyst is necessary.

Table 4.28. Inlet compositions and OSR temperature of the FPP system utilizing 0.25-inch OD reactors

Exp. #	**T_{OSR} (°C)**	**$(W/F)_{OSR}$ (mgcat min/ml)**	**Gas flow rates at OSR feed (ml/min)**				
			CH_4	**O_2**	**H_2O**	**He**	**Total**
1	350	1.68	13.70	9.30	31.10	35.00	89.10
2	350	1.50	13.70	9.30	42.00	35.00	100.00
3	350	1.19	13.70	9.30	68.50	35.00	126.50
4	350	1.07	13.70	9.30	82.60	35.00	140.60
5	400	1.68	13.70	9.30	31.10	35.00	89.10
6	400	1.50	13.70	9.30	42.00	35.00	100.00
7	400	1.19	13.70	9.30	68.50	35.00	126.50
8	400	1.07	13.70	9.30	82.60	35.00	140.60
9	450	1.68	13.70	9.30	31.10	35.00	89.10
10	450	1.50	13.70	9.30	42.00	35.00	100.00
11	450	1.19	13.70	9.30	68.50	35.00	126.50
12	450	1.07	13.70	9.30	82.60	35.00	140.60
13	500	1.68	13.70	9.30	31.10	35.00	89.10
14	500	1.50	13.70	9.30	42.00	35.00	100.00
15	500	1.19	13.70	9.30	68.50	35.00	126.50
16	500	1.07	13.70	9.30	82.60	35.00	140.60

Another constraint for a PEM-grade FP product is to keep the CO level less than 100 ppm; in the simulations, the CO concentration at the exit of FPP was low enough except simulations 15 and 16. It should be noted that “a” attached to simulation number signify that, additional O_2 was added to the system, like in simulation 13-a. At this point it should be noted that in the experimental performance tests O_2 level in the OSR exit is very low, and in some cases, it is practically zero.

Table 4.29. Results of the fuel processor system with 0.25-inch reactor diameter

Exp. #	T_{OSR} (°C)	$(W/F)_{OSR}$ (mgcat min/ml)	H_2 Flow Rate at FPP product (moles/s)	CO level at FPP product (ppm)	X_{CH4} in OSR (%)	X_{CO} in WGS (%)	X_{CO} in PROX (%)
1	350	1.68	6.11×10^{-6}	0.04	50.34	82.99	99.98
2	350	1.50	6.45×10^{-6}	0.01	51.08	94.48	99.98
3	350	1.19	7.81×10^{-6}	0.00	54.10	97.36	99.99
4	350	1.07	7.89×10^{-6}	0.00	53.98	97.98	99.99
5	400	1.68	8.09×10^{-6}	0.08	55.90	84.08	99.98
6	400	1.50	8.95×10^{-6}	0.04	57.99	86.09	99.98
7	400	1.19	1.05×10^{-5}	0.01	61.57	88.07	99.99
8	400	1.07	1.14×10^{-5}	0.01	63.67	91.28	99.99
9	450	1.68	1.15×10^{-5}	0.22	65.39	81.68	99.98
10	450	1.50	1.28×10^{-5}	0.14	68.56	82.99	99.98
11	450	1.19	1.62×10^{-5}	0.15	76.33	83.69	99.98
12	450	1.07	1.82×10^{-5}	0.34	81.41	83.14	99.95
13	500	1.68	1.91×10^{-5}	1444.51	86.30	71.53	75.03
13 – a	500	1.68	1.91×10^{-5}	8.78	86.30	71.53	99.85
14	500	1.50	2.04×10^{-5}	3.38	89.29	73.07	99.92
15	500	1.19	2.44×10^{-5}	223.63	96.91	73.73	93.19
16	500	1.07	2.58×10^{-5}	354.78	98.60	73.91	86.44

In OSR model, as the reaction assumed comprises 5 simultaneous reactions, a 5x5 matrix was created in order to find the selectivities; but, since the matrix was singular, there was no way to find error free results, so the stoichiometric coefficients calculated differed from the real stoichiometric coefficients, and some O_2 may remained unreacted at the exit of OSR. According to the FPP simulation results, O_2 flow at the WGS product is enough to decrease CO level down below 100 ppm at the PROX outlet for all the simulations except simulation 13. This is the reason why additional O_2 was required and added only for simulation 13. On the other extreme, the O_2 level at the entrance of the PROX was so high

for simulations 15 and 16 that the calculated CO level at the PROX exit remained greater than 100 ppm due to negative O_2 order of power law type kinetic expression of PROX slowing down reaction.

It should be noted that, the conversion level in WGS unit in the simulations were between 70-98%, which is higher than expected compared to those obtained in the performance tests for which the conversion did not exceed 70%.

Although the CO concentration levels used at the inlet of WGS reactor during experimental WGS performance tests were 2.1 and 4.9; in the FPP simulations, the CO concentrations calculated at the OSR outlet in 0.13-0.55% range for T_{OSR}=350-450 while reached 1-2% range for T_{OSR}=500 ºC.

The difference between experimental and calculated CO levels for OSR outlet not only yielded higher conversions calculated for WGS reactor, but also very high conversion rates, compared to those obtained in experimental tests, in PROX reactor.

4.2.2. Demo-Fuel Processor System with 1 Inch Reactor Diameter

Demo-FP (DFP) model simulation results presented in Section 4.3.2 showed that, though the FPP having ¼ inch reactors satisfied CO impurity level constraint at the DFP exit, it could only produce H_2 flow levels far lower than needed for 1 kW PEMFC. Thus, in this part of the simulation studies the reactor OD was increased to 1 inch while OSR feed compositions, average residence time (W/F) for the OSR and catalyst bed lengths of all reactors were kept equal to those used in Section 4.2.1. The specifications of the DFP system used in simulations and its inlet conditions were presented in Tables 4.30 and 4.31, respectively. It should be noted that for the DFP simulations, powder form of the catalysts was used though especially for higher bed lengths this may lead to pressure drop during real operation, DFP performance tests. As a consequence of using powder catalyst, the effectiveness factor was taken as 1 for all the OSR, WGS and PROX catalysts for the whole simulation sets.

The results obtained in DFP simulations were tabulated in Table 4.32. The pressure drop values calculated, which are useful in the next section, are also presented as the part of DFP simulation results. It should be noted that for the bed lengths used, the drop calculated in pressure was almost insignificant for FPP system.

Table 4.30. Specifications of the DFP system with 1-inch reactor diameter

Parameter	**Value**	**Unit**
Inner diameter of a reactor	2.12	cm
Total length of a reactor	37	cm
Total length of mixing area	10	cm
Length of O_2 inlet	10	cm
Length of interface areas	1	cm
Length of OSR catalyst bed	1.17	cm
Catalyst amount of OSR reactor	3369	mg
Temperature of OSR reactor	350-500	^oC
Length of WGS catalyst bed	0.485	cm
Catalyst amount of WGS reactor	1684.5	mg
Temperature of WGS reactor	350	^oC
Length of PROX catalyst bed	3.43	cm
Catalyst amount of PROX reactor	5615	mg
Temperature of PROX reactor	110	^oC
Inlet Temperature	25	^oC
Outlet Temperature	25	^oC
Inlet Pressure	1	bar

The results show that in all 16 DFP simulations the molar flow rates of H_2 at DFP outlet are much higher than those obtained in previous section for FPP, although the desired level needed for 1 kW PEMFC was still not reached. On the other hand, for some of the simulations, the results are close to the desired value indicating the additional amount of catalyst necessary should not be significantly higher when effectiveness factor is 1.

The conversion values achieved in OSR are essentially the same as those obtained in FPP simulations owing to the use of same W/F values in both FPP and DFP simulations. On the other hand, decrease in conversion level becomes more significant when the conversions achieved in WGS and PROX reactors of DFP are compared with those of FPP. The results indicate that though the differences in outlet compositions of OSR of FPP and those of DFP are very small for the corresponding simulations, even those slight changes led to significant changes in CO conversions obtained in WGS and PROX reactors of DFP. This is an indication that during practical operations DFP will need precise control for its stable performance even when the perturbations are very small.

Table 4.31. Inlet compositions and OSR temperature of the DFP system with 1-inch reactor diameter

Exp. #	**T_{OSR} (°C)**	**$(W/F)_{OSR}$ (mgcat min/ml)**	**Gas flow rates at OSR feed (ml/min)**				
			CH_4	**O_2**	**H_2O**	**He**	**Total**
1	350	1.68	307.84	208.97	698.82	786.45	2002.08
2	350	1.50	307.84	208.97	943.74	786.45	2247.00
3	350	1.19	307.84	208.97	1539.20	786.45	2842.46
4	350	1.07	307.84	208.97	1856.02	786.45	3159.28
5	400	1.68	307.84	208.97	698.82	786.45	2002.08
6	400	1.50	307.84	208.97	943.74	786.45	2247.00
7	400	1.19	307.84	208.97	1539.20	786.45	2842.46
8	400	1.07	307.84	208.97	1856.02	786.45	3159.28
9	450	1.68	307.84	208.97	698.82	786.45	2002.08
10	450	1.50	307.84	208.97	943.74	786.45	2247.00
11	450	1.19	307.84	208.97	1539.20	786.45	2842.46
12	450	1.07	307.84	208.97	1856.02	786.45	3159.28
13	500	1.68	307.84	208.97	698.82	786.45	2002.08
14	500	1.50	307.84	208.97	943.74	786.45	2247.00
15	500	1.19	307.84	208.97	1539.20	786.45	2842.46
16	500	1.07	307.84	208.97	1856.02	786.45	3159.28

Table 4.32. Results of the fuel processor system with 1-inch reactor diameter

Exp. #	**T_{OSR} (ºC)**	**W/F (mgcat min/ml)**	**FPP exit: P_{out} (bar)**	**FPP exit: Flow Rate of H_2 (moles/s)**	**CO level at FPP product (ppm)**	**X_{CH4} in OSR (%)**	**X_{CO} in WGS (%)**	**X_{CO} in PROX (%)**
1	350	1.68	0.99970	1.34×10^{-4}	40.07	50.34	76.10	87.48
2	350	1.50	0.99966	1.41×10^{-4}	22.65	51.14	87.67	87.52
3	350	1.19	0.99958	1.70×10^{-4}	17.14	54.06	91.42	88.36
4	350	1.07	0.99958	1.71×10^{-4}	14.50	53.91	92.33	87.52
5	400	1.68	0.99974	1.78×10^{-4}	68.50	55.74	77.62	87.48
6	400	1.50	0.99971	1.96×10^{-4}	52.13	57.84	79.36	87.51
7	400	1.19	0.99961	2.28×10^{-4}	31.66	61.51	81.09	87.55
8	400	1.07	0.99959	2.48×10^{-4}	28.99	63.58	84.36	88.05
9	450	1.68	0.99973	2.53×10^{-4}	167.72	65.24	75.74	87.47
10	450	1.50	0.99969	2.80×10^{-4}	138.21	68.42	76.79	87.40
11	450	1.19	0.99955	3.47×10^{-4}	116.70	76.20	77.56	87.55
12	450	1.07	0.99953	3.93×10^{-4}	130.42	81.16	76.88	87.55
13	500	1.68	0.99970	4.16×10^{-4}	2863.75	86.14	66.77	57.44
13 - a	500	1.68	0.99970	4.16×10^{-4}	989.84	86.14	66.77	85.30
14	500	1.50	0.99965	4.45×10^{-4}	640.60	89.09	68.04	87.50
15	500	1.19	0.99958	5.22×10^{-4}	900.34	96.63	68.60	77.03
16	500	1.07	0.99952	5.56×10^{-4}	930.79	98.31	68.80	68.81

Figure 4.2 represents H_2 outlet concentrations at the exit of OSR, WGS and PROX reactors for selected simulation sets performed for different T_{OSR}. Overall evaluation of the results revealed that due to low CO concentrations calculated at the OSR exit for lower OSR temperatures, the contribution of WGS reactor to the H_2 production is essentially insignificant. On the other hand, with the increase in OSR temperatures yielding high CO production, the H_2 produced by WGS become more significant.

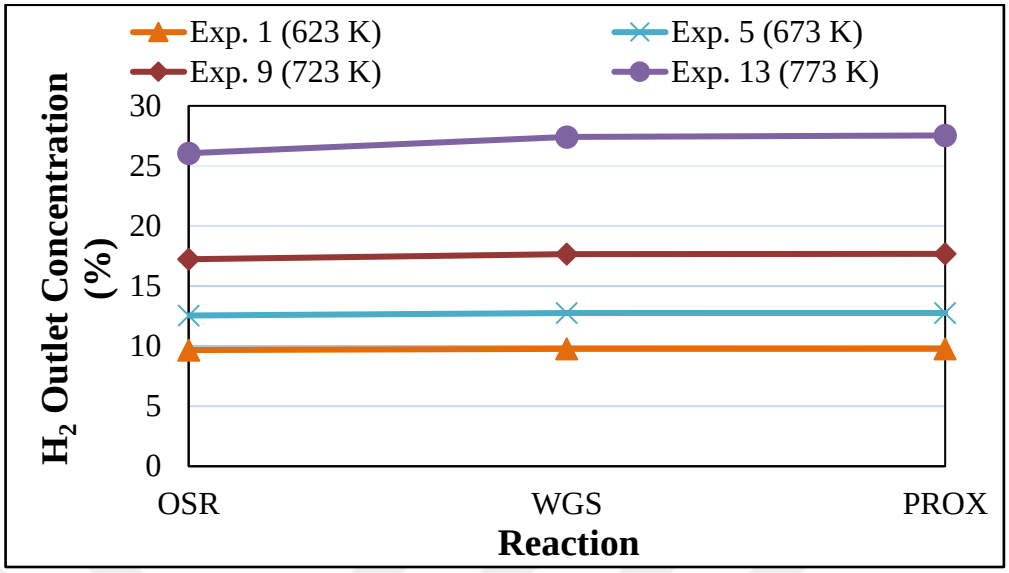

Figure 4.2. H_2 outlet concentration from different reactors in fuel processor system with 1-inch reactor diameter

Figure 4.3 represents CO outlet concentrations at the exit of OSR, WGS and PROX reactors for selected simulation sets performed for different T_{OSR}. The CO production during OSR increases with the increase in OSR temperature. At T_{OSR}=773 K, CO concentration at OSR exit becomes so high that it was not possible to reduce CO concentration to 100 ppm at DFP outlet. The results also show that though most of CO were converted in WGS reactor, it was impossible to reduce the CO concentration at DFP exit to 100 ppm without the PROX reactor.

The results indicated that in several simulations CO amounts were high while in some others H_2 production was too low. At this point, the results of the simulations should be analyzed to find the conditions yielding high FPP performance. As it can be seen from the results presented in Table 4.32, the CO level calculated at the FPP exit for simulations 13, 14, 15 and 16 were already too high even in presence of additional O_2 fed to the system. Besides, considering possible reduced apparent activity due to low effectiveness factor values for granule catalysts will be used in realistic DFP, *which would be significantly less than 1,* the CO level at the DFP exit for the same amounts may be far greater; thus, conditions used for simulation 9, 10, 11 and 12 were also eliminated. Thus, in terms of CO level, the conditions used in first 8 simulations yielding CO level far less than the desired 100 ppm seems reasonable. But, on the other hand, the H_2 production constraint must be also taken

into account. Thus, the simulations have conditions yielding the highest H_2 production rate, ie. simulations 5, 6, 7 and 8, were selected for further analysis, which aims to find the catalyst amounts for a DFP satisfying both H_2 and CO constraints at the same time.

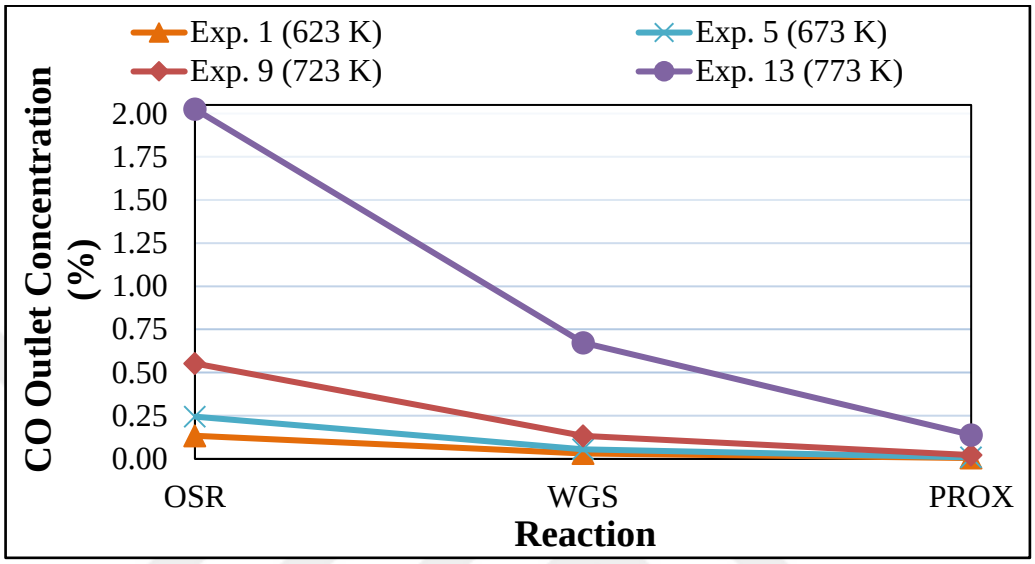

Figure 4.3. H_2 outlet concentration from different reactors in fuel processor system with 1-inch reactor diameter

In the next stage, a preliminary study was conducted by using the Fluent based DFP model aiming to find the amounts of powder catalysts, 0.2Pt-10Ni/δ-Al2O_3, 1Pt-0.5Re-1V/CeO_2 and 1Pt-0.25Sn/AC necessary for OSR, WGS and PROX reactors, respectively, for a DFP satisfying both H_2 and CO constraints under simulations 5-8 conditions; the results are presented in Tables 4.33, 4.34 and 4.35.

Table 4.33. Required OSR catalyst weights to feed 1kW PEMFC

Exp. #	T_{OSR} (°C)	W/F (mgcat min/ml)	Flow Rate of H_2 (moles/s)	Catalyst Weight (mg)	Bed Length (cm)	Pressure Drop (atm)
5	400	1.68	2.72×10^{-3}	49963	17.39	0.0153
6	400	1.50	2.72×10^{-3}	45381	15.80	0.0141
7	400	1.19	2.72×10^{-3}	38879	13.53	0.0137
8	400	1.07	2.72×10^{-3}	35745	12.44	0.0137

Table 4.34. Required WGS catalyst weights to feed 1kW PEMFC

Exp. #	T_{WGS} (°C)	Concentration of CO (ppm)	Catalyst Weight (mg)	Bed Length (cm)	Pressure Drop (atm)
5	350	41.87	24981	7.20	0.00434
6	350	32.09	22691	6.54	0.00350
7	350	20.38	19439	5.60	0.00327
8	350	19.25	17873	5.15	0.00312

Table 4.35. Required PROX catalyst weights to feed 1kW PEMFC

Exp. #	T_{PROX} (°C)	Concentration of CO (ppm)	Catalyst Weight (mg)	Bed Length (cm)	Pressure Drop (atm)
5	110	41.87	83271	50.82	0.07726
6	110	32.09	75635	46.16	0.06442
7	110	20.38	64798	39.55	0.06011
8	110	19.25	59576	36.36	0.05714

In those calculations, the hydrogen flow required at the DFP outlet, 0.00272 moles/s H_2, was assumed achieved in OSR reactor in order to guarantee the DFP satisfy mentioned H_2 flow constraint. As a consequence, WGS an PROX reactors was mainly used to eliminate CO to a level far less than necessary, which is lower than 50 ppm as presented for Table 4.32 for simulations 5-8, in order to guarantee satisfying CO constraint for PEM-grade H_2, ie. maximum 100 ppm at DFP outlet. The results show that the catalyst amounts necessary were less than 50, 25 and 85 grams for OSR, WGS and PROX reactors, respectively, for the conditions applied in simulations 5-8.

4.3. Modeling of OSR: Effect of Catalyst Size and Effectiveness Factor

In this part of the current study, the operation of individual OSR reactor was further simulated for granule-size technical catalyst via introducing several levels of effectiveness factor to the power-law type OSR kinetic expression. In the analysis, the amount of OSR

catalyst, 0.2Pt-10Ni/δ-Al_2O_3, was increased such as to reach the H_2 production level enough to feed 1 kW fuel cell for the conditions used in simulations 5-8. Note that W/F was held constant throughout the analysis. Additionally, particle diameter vs. catalyst bed length and particle diameter vs. pressure drop relations were obtained and analysed.

As the increase in catalyst amount used in a reactor leads to an increase in bed length for a fixed reactor diameter, pressure drop may become a problem for practical applications and should be limited through the use of larger size, ie. granular, catalyst. In the simulations, Ergun's Equation (Equation 4.16) was used to relate the catalyst bed length and pressure drop occurs in the bed. Equation 4.16 also indicate that for the fixed bed length, the diameter of the catalyst must be increased in order to increase voids between particles, bed porosity and permeability, all of which limit the pressure drop.

$$\frac{\Delta P}{L} = \frac{150\,\mu\,u\,(1-\varepsilon)^2}{d_p^2\,\varepsilon^3} + \frac{1.75\,\rho\,u^2(1-\varepsilon)}{d_p\,\varepsilon^3} \tag{4.16}$$

It is safely assumed for powder catalysts that there is no intraparticle mass transfer resistance; as a consequence, the observed rate is the intrinsic rate of reaction. In contrast, with the increase in particle size, the mass transfer resistance becomes significant and lower the apparent reaction rate. In the Fluent based model, effectiveness factor (η), which is the ratio of apparent rate to intrinsic rate (Equation 4.17), was used to modify the intrinsic rate expression for presence of mass transfer resistance (Equation 4.18).

$$\eta = \frac{actual\,rate\,of\,reaction}{intrinsic\,rate\,of\,reaction} \tag{4.17}$$

Upon the addition of effectiveness factor, the actual rate of reaction becomes;

$$-r_{CH_4} = \eta\left[k_0(RT)^{\alpha+\beta+\gamma}e^{\left(\frac{-E_A}{RT}\right)}\right]C_{CH_4}^{\alpha}C_{O_2}^{\beta}C_{H_2O}^{\gamma} \tag{4.18}$$

As there is no apparent rate data collected in performance tests conducted over granular OSR catalysts having different size; in this preliminary work, several effectiveness

factor levels for several possible granule sizes were used in Fluent based OSR model. The particle diameters and corresponding effectiveness factor levels used are presented in Table 4.36.

Table 4.36. Effectiveness factor for different particle diameters

Particle Diameter (μm)	**Effectiveness Factor**
300 (powder)	1
500	1 - 0.8 - 0.6
700	0.9 - 0.7 - 0.5
900	0.8 - 0.6 - 0.4

By using the Fluent based OSR model, the required catalyst amounts and the pressure drop values for the particle diameters and effectiveness factors studied were calculated. The results were presented in three parts; first, the results of the simulations, for which particle diameters were changed while the effectiveness factor level was held constant; then the results of the simulations for which the effectiveness factors were changed while the particle diameter held constant are presented. Finally, all the particle size and effectiveness factor combinations were tabulated. Additionally, the effect of particle diameter to the bed length and pressure drop was studied.

Under simulation 5-8 feed conditions for fixed W/F, the catalyst weights necessary to reach H_2 production level of 2.72 x 10^{-3} moles/s at the exit of the OSR reactor loaded with 300 and 500 μm size catalysts having effectiveness factor 1 along with the pressure drop levels calculated are presented in Table 4.37. Similar results for 500-900 μm size catalyst for η =0.6 are presented in Table 4.38. It is evident that as the particles get larger in size, the bed density is lowered due to increase in bed void fraction. However, the results show that for the particle diameter range studied, the density change with the change in particle size was almost insignificant, and consequently almost the same bed lengths were found in the simulations performed under the same reaction conditions but with different catalyst size (Figure 4.4). On the other hand, the particle diameter had a plausible effect on pressure drop as Ergun Equation suggested; the simulation results show that as the particle diameter was increased, the pressure drop was reduced sharply (Figure 4.5).

Table 4.37. Effect of particle diameter to the catalyst weight and pressure drop with 1 effectiveness factor

Exp. #	Particle Diameter (µm)	Effectiveness Factor	Conversion (%)	Catalyst Weight (mg)	Bed Lenght (cm)	Pressure Drop (atm)
5	300	1	56.18	49963	17.39	0.0153
5	500	1	56.22	49929	17.38	0.0072
6	300	1	58.13	45381	15.80	0.0141
6	500	1	58.13	45381	15.80	0.0066
7	300	1	61.39	38879	13.53	0.0137
7	500	1	61.40	38879	13.53	0.0065
8	300	1	63.59	35745	12.44	0.0137
8	500	1	63.59	35745	12.44	0.0066

Table 4.38. Effect of particle diameter to the catalyst weight and pressure drop with 0.6 effectiveness factor

Exp. #	Particle Diameter (µm)	Effectiveness Factor	Conversion (%)	Catalyst Weight (mg)	Bed Length (cm)	Pressure Drop (atm)
5	500	0.6	55.62	50300	17.51	0.0073
5	900	0.6	55.62	50300	17.51	0.0033
6	500	0.6	57.48	45718	15.92	0.0068
6	900	0.6	57.47	45751	15.93	0.0031
7	500	0.6	60.54	39384	13.71	0.0067
7	900	0.6	60.52	39418	13.72	0.0031
8	500	0.6	61.92	36756	12.80	0.0069
8	900	0.6	61.97	36689	12.77	0.0031

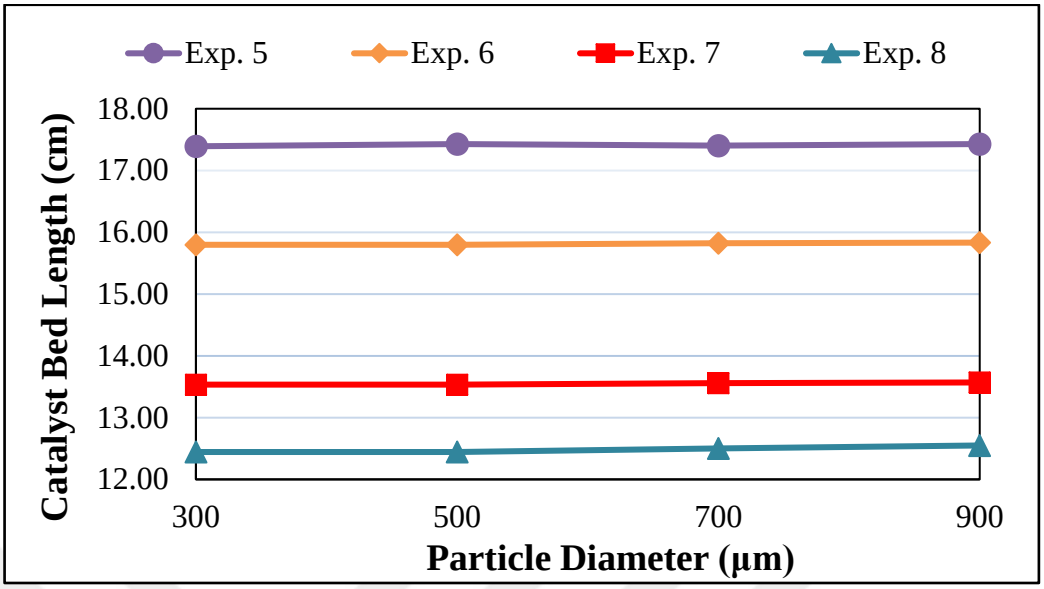

Figure 4.4. Catalyst bed length for different particle diameters

Table 4.39. Effect of effectiveness factor to the catalyst weight and pressure drop with 0.7 µm particle diameter

Exp. #	Particle Diameter (µm)	Effectiveness Factor	Conversion (%)	Catalyst Weight (mg)	Bed Lenght (cm)	Pressure Drop (atm)
5	0.7	0.90	56.13	49996	17.40	0.0045
5	0.7	0.70	55.83	50165	17.46	0.0046
5	0.7	0.50	55.38	50367	17.53	0.0046
6	0.7	0.90	58.07	45448	15.82	0.0043
6	0.7	0.70	57.71	45583	15.87	0.0044
6	0.7	0.50	57.24	45819	15.95	0.0045
7	0.7	0.90	61.23	38946	13.56	0.0041
7	0.7	0.70	60.87	39148	13.63	0.0042
7	0.7	0.50	59.80	39889	13.89	0.0044
8	0.7	0.90	63.31	35914	12.50	0.0042
8	0.7	0.70	62.57	36352	12.65	0.0044
8	0.7	0.50	61.07	37228	12.96	0.0046

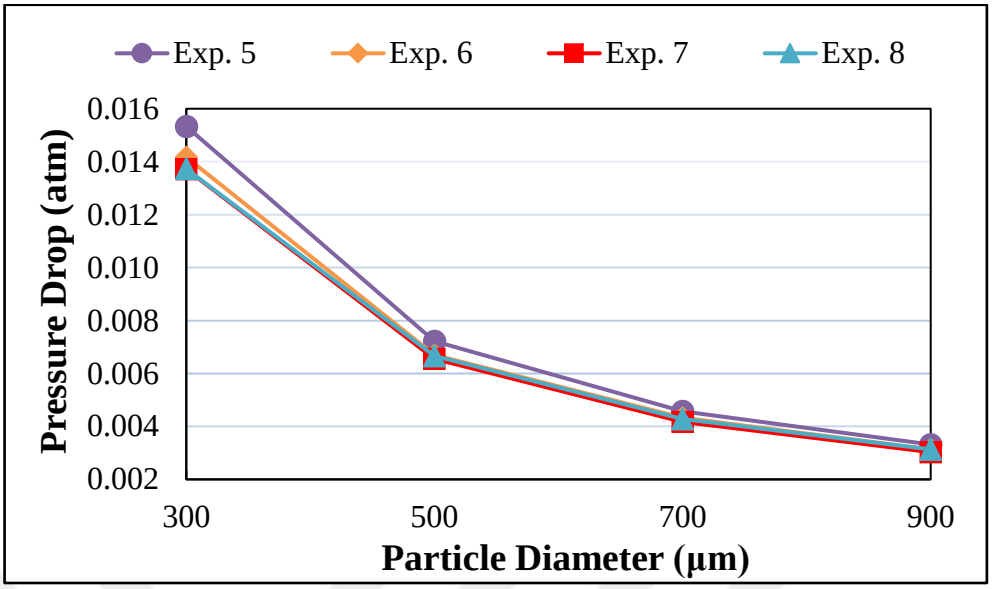

Figure 4.5. Pressure drop for different particle diameters

Table 4.40. Effect of effectiveness factor to the catalyst weight and pressure drop with 0.5 µm particle diameter

Exp. #	Particle Diameter (µm)	Effectiveness Factor	Conversion (%)	Catalyst Weight (mg)	Bed Lenght (cm)	Pressure Drop (atm)
5	0.5	1.00	56.22	49929	17.38	0.0072
5	0.5	0.80	56.00	50064	17.43	0.0072
5	0.5	0.60	55.62	50300	17.51	0.0073
6	0.5	1.00	58.13	45381	15.80	0.0066
6	0.5	0.80	57.90	45482	15.83	0.0067
6	0.5	0.60	57.48	45718	15.92	0.0068
7	0.5	1.00	61.40	38879	13.53	0.0065
7	0.5	0.80	61.00	39081	13.60	0.0066
7	0.5	0.60	60.54	39384	13.71	0.0067
8	0.5	1.00	63.59	35745	12.44	0.0066
8	0.5	0.80	63.07	36049	12.55	0.0067
8	0.5	0.60	61.92	36756	12.80	0.0069

As expected, for the same catalyst size and reaction conditions, the catalyst amount required increases with the decrease in effectiveness factor (Table 4.39 and 4.40), but this increase is rather limited than expected.

5. CONCLUSION

5.1. Conclusions

The main conclusions of the current study can be given as follows:

- The reasons for the mismatch between experimental and calculated conversion values might be stated as follows; firstly, the temperature of the catalyst bed is not equal to outer surface temperature of the reactor due to the heat transfer between catalyst particles. Secondly, in calculating kinetic expression, no effect of porous media was taken into account. A decrease in porosity from 100% means reduced empty spaces between the catalyst particles and it results in reduction in active surface area and ultimately reduces the reaction rate.
- The use of pseudo-inverse function in OSR resulted in ±10% error margin in the extent of reactions. The error in hydrogen stoichiometric coefficients are much less than that of methane stoichiometric coefficients. Therefore, the hydrogen production will be used as the calculation base instead of methane conversion in OSR modeling.
- Performance and modeled results of OSR system were close, the correction factor that minimized the error was obtained as 1.5.
- Performance and modeled results of WGS system were not close. 0.33 correction factor was applied to the kinetic expression. The most probable reasons for the difference is the suppression of conversion during performance tests due to equilibrium nature of the reaction, which exceeds the correction of β' factor at higher conversions.
- Differences between the results of performance tests and porous body effect free Fluent model for the same inlet conditions in PROX hinted that the effect of porosity is small compared to that in OSR and WGS models and no correction factor was applied to the system.
- The highest WGS and PROX conversion values were reached at 350 and 110 ^{o}C, respectively. Therefore, these temperatures were used throughout modeling of the fuel processor system. The catalyst amounts were 75 and 250 mg, respectively.

- In FPP model, some O_2 may remained unreacted at the exit of OSR due to singularity of 5x5 matrix in selectivity of OSR reactions calculation. According to the FPP simulation results, O_2 flow at the WGS product is enough to decrease CO level down below 100 ppm at the PROX outlet for all the simulations except simulation 13. On the other extreme, the O_2 level at the entrance of the PROX was so high for simulations 15 and 16 that the calculated CO level at the PROX exit remained greater than 100 ppm due to negative O_2 order of power law type kinetic expression of PROX slowing down reaction.
- The conversion values achieved in OSR in ¼ inch-OD FPP simulations and 1 inch-OD are essentially the same. On the other hand, decrease in conversion level becomes more significant when the conversions achieved in WGS and PROX reactors of DFP are compared with those of FPP. This is an indication that during practical operations DFP will need precise control for its stable performance even when the perturbations are very small.
- Due to low CO concentrations calculated at the OSR exit for lower OSR temperatures, the contribution of WGS reactor to the H_2 production is essentially insignificant. On the other hand, with the increase in OSR temperatures yielding high CO production, the H_2 produced by WGS become more significant.
- Even though most of CO were converted in WGS reactor, it was impossible to reduce the CO concentration at DFP exit to 100 ppm without the PROX reactor.
- Simulations 5, 6, 7 and 8 yielded the best performance in terms of hydrogen production and CO level at the exit of the PROX reactor were selected.
- The catalyst amounts necessary were less than 50, 25 and 85 grams for OSR, WGS and PROX reactors to satisfy the H_2 flow of 0.00272 moles/s and CO concentration of 100 ppm which are the limit specifications of the Demo-FP outlet for feeding 1 kW PEMFC.
- For the particle diameter range studied, the density change with the change in particle size was almost insignificant, and consequently almost the same bed lengths were found.
- The particle diameter had a plausible effect on pressure drop as Ergun Equation suggested; the simulation results show that as the particle diameter was increased, the pressure drop was reduced sharply.

- For the same catalyst size and reaction conditions, the catalyst amount required increases with the decrease in effectiveness factor, but this increase is rather limited than expected.

5.2. Recommendations

Following ideas can be beneficial for the future studies of modeling a DFC for a 1 kW PEMFC;

- Instead of ANSYS Fluent, a more stable and user-friendly simulation software can be used.
- More performance tests could be performed in order to obtain better simulation results, especially keeping the temperature constant.
- Density and porosity measurements could be done in a more accurate way which will result in more reliable results when the particle size changes.
- Catalysts with smaller particle size would be much more beneficial to study the effect of effectiveness factor if possible.
- A way to measure the temperature within the catalyst would greatly enhance the accuracy of the rate expression if possible.

REFERENCES

Abbas, M. N., "Modeling Of Porosity Equation For Water Flow Through Packed Bed Of Monosize Spherical Packing", *Journal Of Engineering And Development*, Vol. 15, No.4, ISSN 1813- 7822, pp. 205-226, 2011.

Akbari, M. H., A. H. Sharafian Ardakini, and M. Andisheh Tadbir, "A Microreactor Modeling, Analysis and Optimization for Methane Autothermal Reforming in Fuel Cell Applications", *Chemical Engineering Journal*, Vol. 166, pp. 1116-1125, 2011.

Amphlett, J.C., R.F. Mann, B.A. Peppley, "On Board Hydrogen Purification for Steam Reformation/ PEM Fuel Cell Vehicle Power Plants", *International Journal of Hydrogen Energy*, Vol. 21, pp. 673-678, 1996.

Avcı, A. K., Z. I. Önsan, and D. L. Trimm, "On-board Fuel Conversion for Hydrogen Fuel Cells: Comparison of Different Fuels by Computer Simulations", *Applied Catalysis A: General*, Vol. 216, pp. 243-256, 2001.

Barrio, V.L., G. Schaub, M. Rohde, S. Rabe, F. Vogel, J. F. Cambra, P. L. Arias, and M. B. Güemez, "Reactor Modeling to Simulate Catalytic Partial Oxidation and Steam Reforming of Methane. Comparison of Temperature Profiles and Strategies for Hot Spot Minimization", *International Journal of Hydrogen Energy*, Vol. 32, pp. 1421-1428, 2007.

Başar, M. S., H. Bedir, and A. E. Aksoylu, "Steady State Performance Analysis of OSR and Serial OSR-WGS Reactors", *Fuel Processing Technology*, Vol. 152, pp. 240-249, 2016.

Başar M. S., B. S. Çağlayan, A. E. Aksoylu, "A Study on Catalytic Hydrogen Production: Thermodynamic and Experimental Analysis of Serial OSR-PROX System", in progress.

Berry, G. D., “Hydrogen Production”, *Encyclopedia of Energy*, 6th ed. Elsevier, 2004.

Carman, P. C., “Permeability of Saturated Sands, Soils and Clays”, *The Journal of Agricultural Science*, Vol. 27, pp. 262-273, 1938.

Choi, Y., and H.G. Stenger, “Water Gas Shift Reaction Kinetics and Reactor Modeling for Fuel Cell Grade Hydrogen”, *Journal of Power Sources*, Vol. 124, pp. 432-439, 2003.

Chrenko, D., F. Gao, B. Blunier, D. Bouquain, and A. Miraoui, “Methanol Fuel Processor and PEM Fuel Cell Modeling for Mobile Application”, *International Journal of Hydrogen Energy*, Vol. 35, pp. 6863-687, 2010.

Çağlayan, B. S., I. I. Soykal, A. E. Aksoylu, “Preferential Oxidation of CO over Pt–Sn/AC Catalyst: Adsorption, Performance and DRIFTS Studies”, *Applied Catalysis B: Environmental*, Vol. 106, pp. 540-549, 2011.

EG&G Technical Services, Inc., *Fuel Cell Handbook*, 7th ed., U.S. Department of Energy, West Virginia, 2004.

Ergun, S., “Fluid Flow through Packed Columns”, *Chemical Engineering Progress*, Vol. 48, No.2, pp. 89-94, 1952.

Eropak, B. M., A. E. Aksoylu, “A Reliable Power-Law Type Kinetic Expression for PROX over Pt-Sn/AC under Fully Realistic Conditions”, *Catalysis Communications*, Vol. 95, pp. 67-71, 2017.

Feng, C.L. and A.U. Yu, “Effect of Liquid Addition on The Packing of Mono-Sized Coarse Spheres”, *Powder Technology*, Vol. 99, pp. 22-28, 1998.

Froment, G.F., and K.B. Bischoff, *Chemical Reactor Analysis and Design*, Second ed., Wiley, New York, 1990.

Fuel Cell Today, *Fuel Cell Basics, Technology Types*, 2012.

Furnas, C. C., “Grading Aggregates I-Mathematical Relations for Beds of Broken Solids of Maximum Density”, *Industrial & Engineering Chemistry*, Vol. 23, pp. 1052-1058, 1931.

Holladay, J.D., and Y. Wang, “A Review of Recent Advances in Numerical Simulations of Microscale Fuel Processor for Hydrogen Production”, *Journal of Power Sources*, Vol. 282, pp. 602-621, 2015.

Hong, J., W. C. Hecker and T. H. Fletcher, *Predicting Effectiveness Factor for M-th Order and Langmuir Rate Equations in Spherical Coordinates*, Chemical Engineering Department, Brigham Young University, Provo, 1999.

Idel’chik, I.E., *Handbook of Hydraulic Resistance*, Gosudarstvennoe Energeticheskoe Izdatel'stvo, Moskva-Leningrad, 1960.

Jin, W., X. Gu, S. Li, P. Huang, N. Xu, and J. Shi, “Experimental and Simulation Study on a Catalyst Packed Tubular Dense Membrane Reactor for Partial Oxidation of Methane to Syngas”, *Chemical Engineering Science*, Vol. 55, pp. 2617-2625, 2000.

Johnston, B., M. C. Mayo, and A. Khare, “Hydrogen: The Energy Source for the 21st Century”, *Technovation*, Vol. 25, pp. 569-585, 2005.

Kaundinya, D. P., P. Balachandra, and N. H. Ravindranath, “Grid-Connected Versus Stand-Alone Energy Systems for Decentralized Power - A Review of Literature”, *Renewable and Sustainable Energy Reviews*, Vol. 13, pp. 2041-2050, 2009.

Keiski, R.L., O. Desponds, Y. F. Chang, G. A. Somorjai, “Kinetics of The Water-Gas Shift Reaction over Several Alkane Activation and Water-Gas Shift Catalysts”, *Applied Catalysis A*, Vol. 101, pp. 317-338, 1993.

Kesim, B., *An Experimental Study on Optimization of Pt-Based Trimetallic WGS Catalysts*, M. S. Thesis, Boğaziçi University, 2017.

Lattner, J.R., and M. P. Harold, “Comparison of Methanol-Based Fuel Processors for PEM Fuel Cell Systems”, *Applied Catalysis B: Environmental*, Vol. 56, pp. 149-169, 2005.

Leva, M., M. Weinfraub, M. Grummer, M. Pollchik, and H. H. Sforch, *Fluid Flow through Packed and Fluidized Systems*, United States Government Printing Office, Washinqton, 1951.

Lin, S.T., Y. H. Chen, C. C. Yu, Y. C. Liu, and C. H. Lee, “Modelling an Experimental Methane Fuel Processor”, *Journal of Power Sources*, Vol. 148, pp. 43-53, 2005.

Lin, S.T., Y. H. Chen, C. C. Yu, Y. C. Liu, and C. H. Lee, “Dynamic Modeling and Control Structure Design of an Experimental Fuel Processor”, *International Journal of Hydrogen Energy*, Vol. 31, pp. 413-426, 2006.

Löffler, D.G., K. Taylor, and D. Mason, “A Light Hydrocarbon Fuel Processor Producing High-Purity Hydrogen”, *Journal of Power Sources*, Vol. 117, pp. 84-91, 2003.

Ma, L., D. L. Trimm, and C. Jiang, “The Design and Testing of an Autothermal Reactor for the Conversion of Light Hydrocarbons to Hydrogen I: The Kinetics of the Catalytic Oxidation of Light Hydrocarbons”, *Applied Catalysis A: General*, Vol. 138, pp. 275-283, 1996.

Mariño F., C. Descorme, D. Duprez, “Noble Metal Catalysts for the Preferential Oxidation of Carbon Monoxide in the Presence of Hydrogen (PROX)”, *Applied Catalysis B: Environmental*, Vol. 54, pp. 59-66, 2004.

Maklavany, D. M., A. Shariati, B. Roozbehani, and M. R. Khosravi Nikou, “Kinetic Modeling of Low Temperature Water-Gas Shift Reaction Using Gproms”, *American Journal of Oil and Chemical Technologies*, Vol. 4., Issue 2, pp. 70-80, 2016.

Mota, M., J. A. Teixeira, A. Yelshin, “Image Analysis of Packed Beds of Spherical Particles of Different Sizes”, *Separation and Purification Technology*, Vol. 15, pp. 59-68, 1999.

Natesakhawat, S., X. Wang, L. Zhang and U. S. Ozkan, “Development of Chromium-Free Iron-Based Catalysts for High-Temperature Water-Gas Shift Reaction”, *Journal of Molecular Catalysis A: Chemical*, Vol. 260, pp. 82-94, 2006.

Newsome, D., “The Water - Gas Shift Reaction”, *Catalysis Reviews - Science and Engineering*, Vol. 21, pp. 275-318, 1980.

Pacheco, M., J. Sira, and J. Kopasz, “Reaction Kinetics and Reactor Modeling for Fuel Processing of Liquid Hydrocarbons to Produce Hydrogen: Isooctane Reforming”, *Applied Catalysis A: General*, Vol. 250, pp. 161-175, 2003.

Peppley, B.A., J.C. Amphlett, L.M. Kearns, and R.F. Mann, “Methanol-Steam Reforming on $Cu/ZnO/Al_2O_3$ Catalysts. Part 2. A Comprehensive Kinetic Model”, *Applied Catalysis A: General*, Vol. 179, pp. 31-49, 1999.

Pushnov, A. S., “Calculation of Average Bed Porosity”, *Chemical and Petroleum Engineering*, Vol. 42, Nos. 1-2, pp. 14-17, 2006.

Qi, A., B. Peppley, and K. Karan, “Integrated Fuel Processors for Fuel Cell Application: A Review”, *Fuel Processing Technology*, Vol. 88, pp. 3-22, 2007.

Rawlings, J. B., J. G. Ekerdt, *Chemical Reactor Analysis and Design Fundamentals*, 2nd Edition, Ch. 7, 2015.

Ramani V., “Fuel Cells”, *The Electrochemical Society*, pp. 41-44, 2006.

Reitz, T. L., S. Ahmed, M. Krumpelt, R. Kumar, H. H. Kung, “Characterization of CuO/ZnO under Oxidizing Conditions for the Oxidative Methanol Reforming Reaction”, *Journal of Molecular Catalysis A: Chemical*, Vol. 162, pp. 275-285, 2000.

Rostrup-Nielsen, *Catalytic steam reforming, in: John Anderson, Michel Boudart (Ed.),* Catalysis Science and Technology, Chapter 1, Springer, 1984.

Salemme, L., L. Menna, and M. Simeone, *Energy efficiency of Fuel Processor – PEM Fuel Cell systems*, Energy Efficiency, Jenny Palm (Ed.), ISBN: 978-953-307-137-4, InTech, 2010.

Shekhawat, D., J. J. Spivey, and D. A. Berry, *Fuel Cells: Technologies for Fuel Processing*, Elsevier, Amsterdam, pp. 73-128, 2011.

Silva Herran, D., and T. Nakata, "Design of Decentralized Energy Systems for Rural Electrification in Developing Countries Considering Regional Disparity", *Applied Energy*, Vol. 91, pp. 130-145, 2012.

Smith, B. R. J., M. Loganathan, and M. S. Shantha, "A Review of the Water Gas Shift Reaction Kinetics", *International Journal of Chemical Reactor Engineering*, Vol. 8, 2010.

Trimm, D.L., and C. Lam, "The Combustion of Methane on Platinum–Alumina Fiber Catalysis I: Kinetics and Mechanism", *Chemical Engineering Science*, Vol. 35, pp. 1405-1413, 1980.

Westbrook, C.K. and F.L. Dryer, "Simplified Reaction Mechanisms for the Oxidation of Hydrocarbon Fuels in Flames", *Combustion Science and Technology*, Vol. 27, pp. 31-43, 1981.

Xu, J., and G. F. Froment, "Methane Steam Reforming, Methanation and Water - Gas Shift I: Intrinsic Kinetics", *AIChE Journal*, Vol. 35, pp. 88-96, 1989.

Yumru, G., *WGS Kinetics over Pt-Based Trimetallic Catalyst under Realistic Conditions*, M. S. Thesis, Boğaziçi University, 2017.

Zahedi, N. M., S. Rowshanzamir, and M. H. Eikani, "Autothermal Reforming of Methane to Synthesis Gas: Modeling and Simulation", *International Journal of Hydrogen Energy*, Vol. 34, pp. 1292-1300, 2009.